# Global Soundings of the Atmosphere from ATOVS Measurements: The Algorithm and Validation

JUN LI AND WALTER W. WOLF

*Cooperative Institute for Meteorological Satellite Studies, Space Science and Engineering Center, University of Wisconsin—Madison, Madison, Wisconsin*

W. PAUL MENZEL

*Office of Research and Application, National Oceanic and Atmospheric Administration, National Environmental Satellite, Data, and Information Service, Madison, Wisconsin*

WENJIAN ZHANG

*National Satellite Meteorological Center, China Meteorological Administration, Beijing, China*

HUNG-LUNG HUANG AND THOMAS H. ACHTOR

*Cooperative Institute for Meteorological Satellite Studies, Space Science and Engineering Center, University of Wisconsin—Madison, Madison, Wisconsin*

(Manuscript received 2 July 1999, in final form 5 November 1999)

ABSTRACT

The International Advanced Television and Infrared Observation Satellite Operational Vertical Sounder (ATOVS) Processing Package (IAPP) has been developed to retrieve the atmospheric temperature profile, moisture profile, atmospheric total ozone, and other parameters in both clear and cloudy atmospheres from the ATOVS measurements. The algorithm that retrieves these parameters contains four steps: 1) cloud detection and removal, 2) bias adjustment for ATOVS measurements, 3) regression retrieval processes, and 4) a nonlinear iterative physical retrieval. Nine ($3 \times 3$) adjacent High-Resolution Infrared Sounder (HIRS)/3 spot observations, together with Advanced Microwave Sounding Unit-A observations remapped to the HIRS/3 resolution, are used to retrieve the temperature profile, moisture profile, surface skin temperature, total atmospheric ozone and microwave surface emissivity, and so on. ATOVS profile retrieval results are evaluated by root-mean-square differences with respect to radiosonde observation profiles. The accuracy of the retrieval is about 2.0 K for the temperature at 1-km vertical resolution and 3.0–6.0 K for the dewpoint temperature at 2-km vertical resolution in this study. The IAPP is now available to users worldwide for processing the real-time ATOVS data.

## 1. Introduction

The Advanced Microwave Sounding Unit (AMSU) on the *NOAA-15* satellite, has a total of 20 channels in the microwave; this represents a dramatic improvement in microwave technology over the Microwave Sounding Unit (MSU) from the Television and Infrared Observation Satellite (TIROS)-N Operational Vertical Sounder (TOVS) (Smith et al. 1979). The Advanced TOVS (ATOVS) is composed of Advanced Microwave Sounding Unit (AMSU) and High-Resolution Infrared Sounder (HIRS)/3, and flies on the National Oceanic and Atmospheric Administration (NOAA) polar-orbiting satellite (*NOAA-15*) launched on 13 May 1998. Two separate radiometers (AMSU-A and AMSU-B) compose the AMSU platform. The AMSU-A is a cross-track, stepped-line scanning total power radiometer. The instrument has an instantaneous field-of-view of 3.3° at the half-power points providing a nominal spatial resolution at nadir of 48 km. The AMSU-B is a cross-track, continuous line scanning, total power radiometer with an instantaneous field-of-view of 1.1° (at the half-power points). Spatial resolution at nadir is nominally 16 km. The antenna provides a cross-track scan, scanning $\pm 48.95°$ from nadir with a total of 90 earth fields-of-view per scan line. The instrument completes one

*Corresponding author address:* Dr. Jun Li, Rm. 219, CIMSS/SSEC, University of Wisconsin—Madison, 1225 West Dayton Street, Madison, WI 53706.
E-mail: junl@ssec.wisc.edu

TABLE 1. AMSU-A channel characteristics.

| Channel No. | Center frequency | No. of pass bands | Bandwidth (MHz) | Center frequency stability (MHz) | Temperature sensitivity (K) NE$\Delta$T | Calibration accuracy (K) | Angle $\theta$p |
|---|---|---|---|---|---|---|---|
| 1 | 23 800 MHz | 1 | 270 | 10 | 0.3 | 2.0 | V |
| 2 | 31 400 MHz | 1 | 180 | 10 | 0.3 | 2.0 | V |
| 3 | 50 300 MHz | 1 | 180 | 10 | 0.4 | 1.5 | V |
| 4 | 52 800 MHz | 1 | 400 | 5 | 0.25 | 1.5 | V |
| 5 | 53 596 $\pm$ 115 MHz | 2 | 170 | 5 | 0.25 | 1.5 | H |
| 6 | 54 400 MHz | 1 | 400 | 5 | 0.25 | 1.5 | H |
| 7 | 54 940 MHz | 1 | 400 | 5 | 0.25 | 1.5 | V |
| 8 | 55 500 MHz | 1 | 330 | 10 | 0.25 | 1.5 | H |
| 9 | 57 290.344 MHz = $f_{LO}$ | 1 | 330 | 0.5 | 0.25 | 1.5 | H |
| 10 | $f_{LO}$ $\pm$217 MHz | 2 | 78 | 0.5 | 0.4 | 1.5 | H |
| 11 | $f_{LO}$ $\pm$ 322.2 $\pm$ 48 MHz | 4 | 36 | 1.2 | 0.4 | 1.5 | H |
| 12 | $f_{LO}$ $\pm$ 322.2 $\pm$ 22 MHz | 4 | 16 | 1.2 | 0.6 | 1.5 | H |
| 13 | $f_{LO}$ $\pm$ 322.2 $\pm$ 10 MHz | 4 | 8 | 0.5 | 0.80 | 1.5 | H |
| 14 | $f_{LO}$ $\pm$ 322.2 $\pm$ 4.5 MHz | 4 | 3 | 0.5 | 1.20 | 1.5 | H |
| 15 | 89.0 GHz | 1 | 6 000 | 50 | 0.5 | 2.0 | V |

scan every 2.66 s. Tables 1 and 2 list the AMSU-A and AMSU-B channel characteristics.

The primary function of the 15-channel AMSU-A (channels 1–15) is to provide temperature sounding of the atmosphere; three of the channels will also provide information on tropospheric water vapor, precipitation over ocean, sea-ice coverage, and other surface characteristics. The five channels of the AMSU-B (channels 16–20) mainly measure water vapor and liquid precipitation over land and sea. For the first time with AMSU, global profiling of atmospheric temperature and moisture in all weather conditions is possible. In a clear atmosphere, the major absorbing constituents in AMSU channels are oxygen and water vapor. Figure 1 shows the AMSU-A sensitivity functions ($d\tau/d\ln p$); it can be seen that there are several channels (channels 9–14) that have good sensitivity for stratospheric temperature information.

Another instrument of ATOVS is the HIRS/3. The HIRS/3 is a 20 channel instrument that has an instantaneous field-of-view of 1.3° providing a nominal spatial resolution at nadir of 18.9 km. The antenna provides a cross-track stepped scan, scanning $\pm$49.5° from nadir with a total of 56 fields-of-view per scan. The instrument completes one scan line every 6.4 s. Table 3 lists the HIRS/3 channel characteristics. Figure 2 shows the HIRS/3 weighting functions; it can be seen that the information is concentrated in the troposphere for the infrared channels. Data from the HIRS/3 instrument is used, in conjunction with the AMSU instruments, to calculate the atmospheric vertical temperature profile from the earth's surface to about 40-km altitude.

The International ATOVS Processing Package (IAPP) has been developed at the University of Wisconsin—Madison and is now available to the users worldwide for processing real-time ATOVS data. A simulation study of the IAPP was carried out for the algorithm development (Li et al. 1998b). In this paper, the algorithm for ATOVS real data processing is presented. The retrieval algorithm for ATOVS data processing is composed of four steps: 1) HIRS/3 cloud detection and removal of cloud effects; 2) bias correction for the HIRS/3 radiative transfer calculations; 3) regression solution for parameters to be retrieved; and 4) nonlinear iterative physical retrieval of the atmospheric temperature profile, moisture profile, atmospheric total ozone, surface skin temperature and microwave surface emissivity through solving the radiative transfer equation (RTE). In the IAPP algorithm, the AMSU-A measurements are remapped to the HIRS/3 field-of-view (FOV) and the retrieval processing is based on a field-of-regard (FOR) containing 3 $\times$ 3 adjacent HIRS/3 FOVs; hereinafter a

TABLE 2. AMSU-B channel characteristics.

| | | Bandwidth | | | |
|---|---|---|---|---|---|
| Channel No. | Center frequency (GHz) | Double-sided max (MHz) | Pass band (MHz) | IF band (MHz) | Stop band (MHz) |
| 16 | 89.0 | 6000 | 3000 | $\geq$1000 | $\pm$400 |
| 17 | 150.0 | 4000 | 2000 | $\geq$1000 | $\pm$400 |
| 18 | 183.31 $\pm$ 1.0 | 1000 | 2 $\times$ 500 | 500 | — |
| 19 | 183.31 $\pm$ 3.0 | 2000 | 2 $\times$ 1000 | 1000 | — |
| 20 | 183.31 $\pm$ 7.0 | 4000 | 2 $\times$ 2000 | 2000 | — |

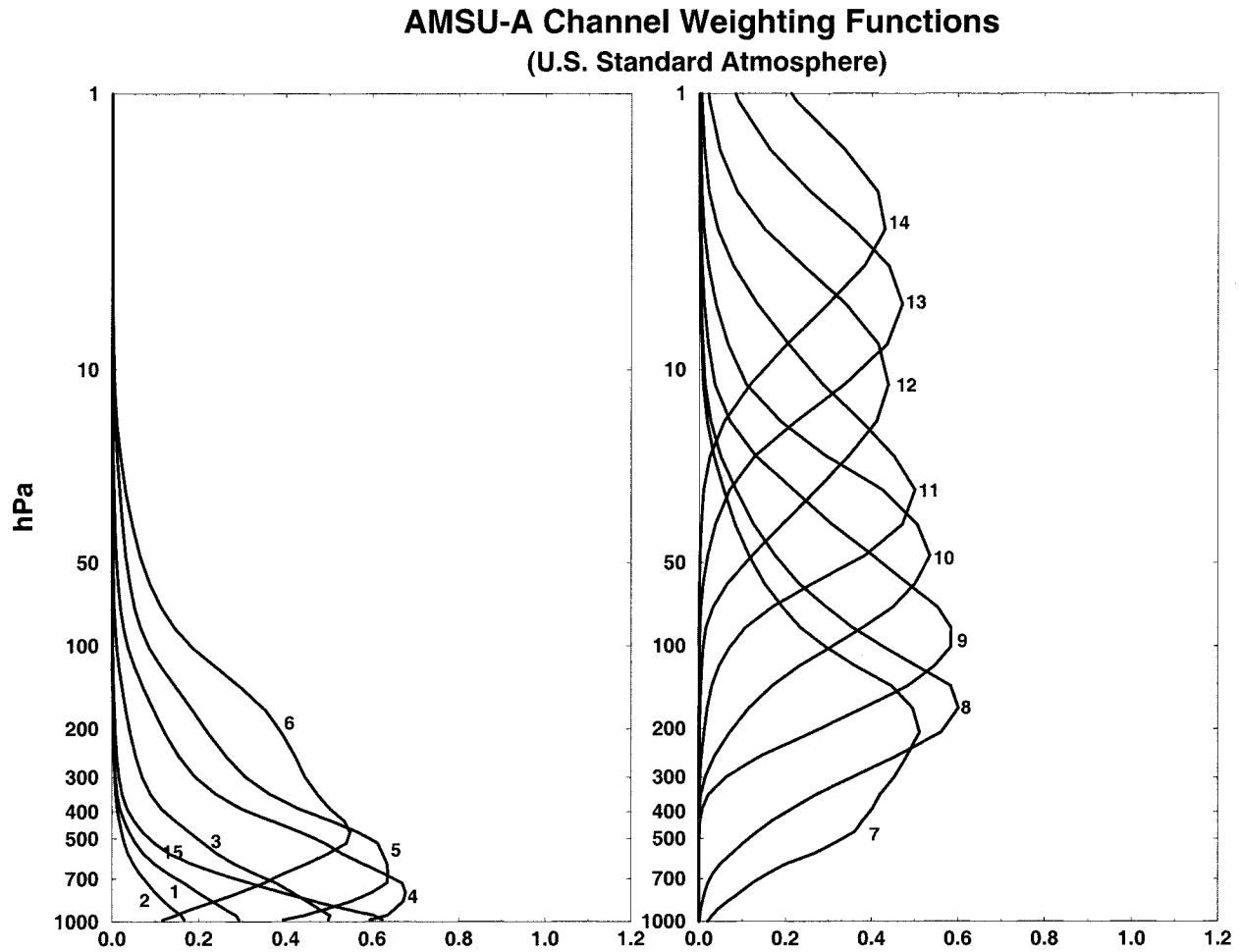


FIG. 1. AMSU-A sensitivity functions ($d\tau/d\ln p$).

FOR is always defined as the 3 × 3 adjacent HIRS/3 FOVs. The retrieval results are compared with radiosonde observation (raob) profiles. Case studies for 15 and 16 November 1998 show that the ATOVS measurements are capable of capturing the main structure of the atmospheric profile. Retrieval results are evaluated by the root mean square (rms) differences between the retrieved ATOVS and the collocated raob profiles. Statistical rms errors of temperature and dewpoint temperature show that the accuracy of the IAPP retrieval is about 2.0 K for temperature at 1-km vertical resolution and 3–6 K for dewpoint temperature at 2-km vertical resolution. Currently, because of communication interference problems, the AMSU-B data are not used in this study because the calibration correction needs to be improved for retrieval processing. When an accurate calibration is achieved, the water vapor retrieval is expected to be improved by using AMSU-B measurements.

Section 2 describes the forward model and bias correction for the forward model, a cloud detection and removal scheme is outlined in section 3, and the retrieval algorithm for ATOVS processing is detailed in sections 4 and 5. Quality control for the retrievals is described in section 6. Last, the validation of the retrieval analysis is described in section 7.

## 2. Forward model and bias adjustment

To determine the retrieval accuracy, a precise knowledge of the instrument performance and the accuracy of the atmospheric transmittance functions for the various spectral channels are crucial. In the IAPP, a fast and accurate transmittance model is generated for the RTE calculation; it is called Pressure Layer Optical Depth (PLOD) (Hannon et al. 1996) and uses 42 pressure level vertical coordinates from 0.1 to 1050 hPa. Uncertainty associated with the infrared surface emissivity, surface skin temperature, and the transmittance model can be evaluated with a matchup file, which contains the time and space collocated satellite observations and radiosonde profiles (Zhang et al. 1999). The criteria for selecting ATOVS measurements with collocated radiosonde data are based on the following.

TABLE 3. HIRS/3 channel characteristics (for channel 20, A is albedo).

| Channel No. | Channel frequency ($cm^{-1}$) | Band ($\mu$m) | Half-power bandwidth ($cm^{-1}$) | Anticipated max scene temperature (°) | Specified sensitivity* | Design goal |
|---|---|---|---|---|---|---|
| 1 | 669 | 14.95 | 3 | 280 | 3.00 | 0.75 |
| 2 | 680 | 14.71 | 10 | 265 | 0.67 | 0.25 |
| 3 | 690 | 14.49 | 12 | 240 | 0.50 | 0.25 |
| 4 | 703 | 14.22 | 16 | 250 | 0.31 | 0.20 |
| 5 | 716 | 13.97 | 16 | 265 | 0.21 | 0.20 |
| 6 | 733 | 13.64 | 16 | 280 | 0.24 | 0.20 |
| 7 | 749 | 13.35 | 16 | 290 | 0.20 | 0.20 |
| 8 | 900 | 11.11 | 35 | 330 | 0.10 | 0.10 |
| 9 | 1030 | 9.71 | 25 | 270 | 0.15 | 0.15 |
| 10 | 802 | 12.47 | 16 | 300 | 0.15 | 0.10 |
| 11 | 1365 | 7.33 | 40 | 275 | 0.20 | 0.20 |
| 12 | 1533 | 6.52 | 55 | 255 | 0.20 | 0.07 |
| 13 | 2188 | 4.57 | 23 | 300 | 0.006 | 0.002 |
| 14 | 2210 | 4.52 | 23 | 290 | 0.003 | 0.002 |
| 15 | 2235 | 4.47 | 23 | 280 | 0.004 | 0.002 |
| 16 | 2245 | 4.45 | 23 | 270 | 0.004 | 0.002 |
| 17 | 2420 | 4.13 | 28 | 330 | 0.002 | 0.002 |
| 18 | 2515 | 4.00 | 35 | 340 | 0.002 | 0.002 |
| 19 | 2660 | 3.76 | 100 | 340 | 0.001 | 0.001 |
| 20 | 14 500 | 0.69 | 1 000 | 100%A | 0.10% A | — |

* NE$\Delta$N (mW $m^{-2}$ Sr $cm^{-1}$).

1) The collocation is based on the IAPP retrieval FOR ($3 \times 3$ FOVs) and the nearest collocated radiosonde observations in both time and space.
2) The absolute distance between the position (latitude and longitude) of the radiosonde and the ATOVS retrieval FOR is less than 1.0° (the central FOV is chosen to represent the position of the ATOVS retrieval FOR).
3) The time difference between radiosonde and ATOVS measurements is less than 1.5 h.
4) The satellite zenith angle of the ATOVS measurement is less than 25°.
5) The cloud check procedure described in section 3 is applied to each FOR; only clear FORs are used in comparisons.
6) Only FORs with minimal topography variation are selected.

Based on these criteria, a global collocated dataset has been generated with more than 1500 clear collocated samples from 3 September 1998 to 9 March 1999. Empirical corrections for discrepancies are made with a bias vector that can be added to the measured brightness temperatures (Fleming et al. 1986; Hayden 1988). The ATOVS measurements are compared with those from the forward calculations using the radiosonde profiles mentioned above. The surface skin temperature used in the calculation is obtained through a regression from the HIRS/3 longwave window channels (11.11 and 12.47 $\mu$m) during nighttime conditions, while longwave window channels plus shortwave window channel (4.00 $\mu$m) are used for daytime conditions. If the surface temperature observation is provided, the surface skin temperature is determined from regression by using both the HIRS/3 window channels and the surface temperature observation. The ATOVS measurements of each FOR are averaged to reduce the noise. If the calculations are shown to have systematic bias from the ATOVS measurements, then the bias correction can be applied in retrieval processing.

Bias corrections are calculated for most of the HIRS/3 and AMSU-A channels. Figure 3 shows the scattering plot of observed and calculated brightness temperatures for HIRS/3 channels 5, 6, 7, and 8. Clearly, channels 5, 6, and 7, which are the principle temperature sounding channels, all have correlations in excess of 0.98. However, the correspondence between observed and calculated brightness temperatures for window channel 8 is not very good due to the fact that channel 8 is mainly sensitive to the surface skin temperature. Figure 4 is the same as Fig. 3 but for AMSU-A channels 4, 5, 6, and 7. The correlation between observed and calculated values for channel 4 is also not very good since this channel is sensitive to the surface emissivity, while channels 5, 6, and 7, which are the microwave temperature sounding channels, have good correlations. In general there is good agreement between the calculations and observations; the systematic bias error between the calculations and measurements can be derived and adjusted in the retrieval. The bias correction can be carried out by either adjusting the ATOVS observation or the forward model calculation. In the IAPP, the ATOVS measurements are adjusted for use in the retrieval procedure; the adjusted brightness temperature is expressed as:

$$T_B^* = aT_B + b, \tag{1}$$

where the $T_B^*$ is the adjusted ATOVS brightness tem-

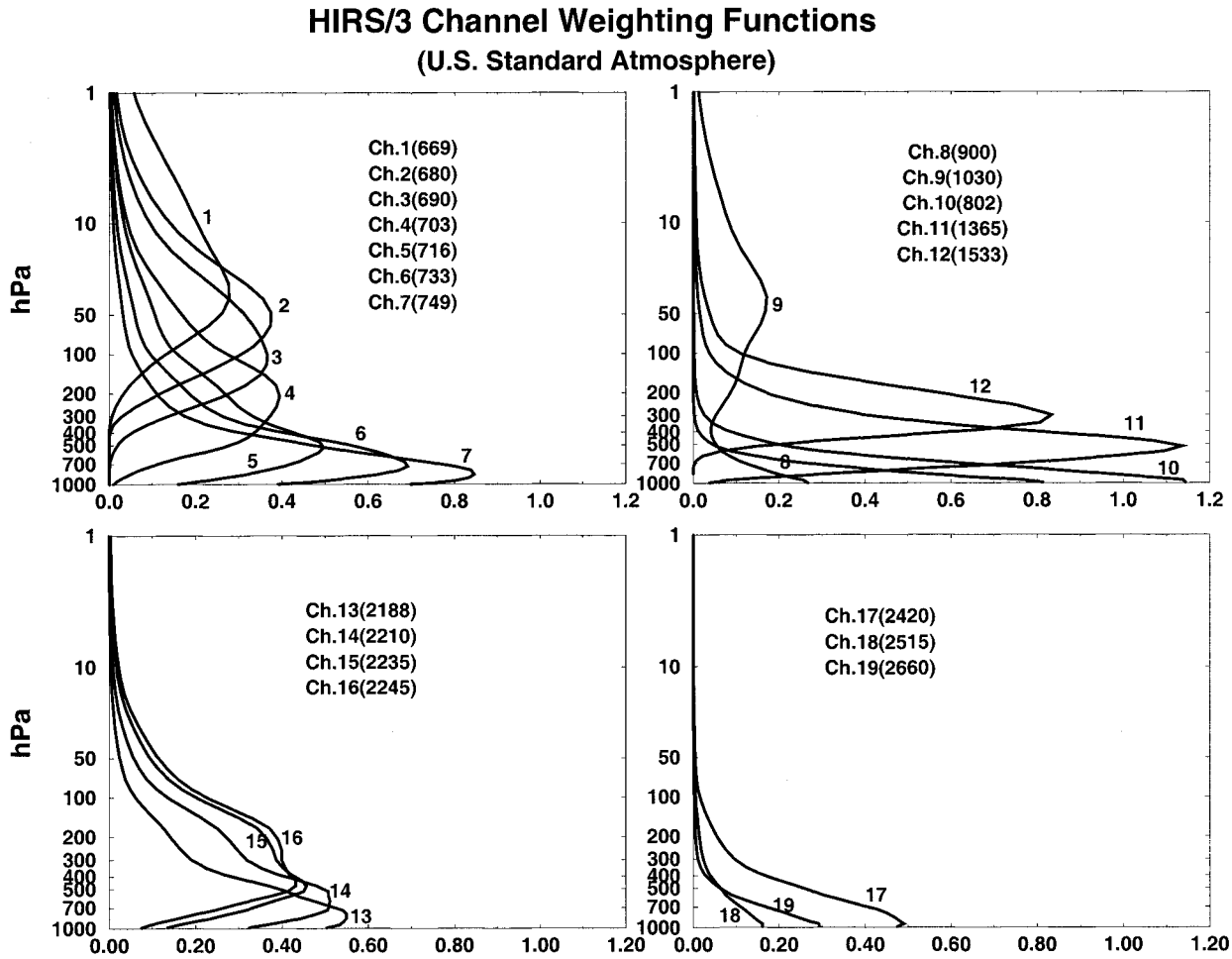


FIG. 2. HIRS/3 sensitivity functions ($d\tau/d\ln p$).

perature and $T_B$ is the original observed brightness temperature for a given channel, $a$ and $b$ are the slope and intercept coefficients, respectively, which are calculated from the matchup file mentioned above. Table 4 lists the slope and intercept coefficients for HIRS/3 and AMSU-A channels. The HIRS/3 channel-9 bias adjustment is not applied because there are no ozone profiles in the matchup file. Also the bias adjustment for AMSU-A window channels 1–3 and 15 are not applied because there are microwave surface emissivity uncertainties in the calculations. Figure 5 shows the comparisons between observed AMSU-A channel-5 brightness temperatures and calculated brightness temperatures from collocated radiosonde profiles. The blue and red spots in this figure are before and after bias adjustments respectively; obviously the systematic bias is removed after adjustment.

## 3. Cloud detection and cloud removal procedure for HIRS/3

An integral part of the retrieval algorithm is the detection of cloud contamination with special consideration of HIRS/3 measurement characteristics. For each HIRS/3 FOV, a cloud detection algorithm is applied to get the clear/cloudy index. A number of cloud detection schemes have been implemented for HIRS/2 data processing (Smith et al. 1979; McMillin and Dean 1982). These schemes are applied to the HIRS/3 data processing. In addition, AMSU-A measurements are used for HIRS/3 cloud detection. In the retrieval processing, AMSU-A measurements for channels 4–14 are used to predict HIRS/3 brightness temperatures. The differences between observed and AMSU-A predicted HIRS/3 brightness temperatures are also used for cloud detection.

The HIRS/3 cloud detection algorithm is outlined in Fig. 6. The input data include the brightness temperatures of all HIRS/3 channels where each FOV undergoes the following general tests:

1) *Longwave window channel (11.11 μm) brightness temperature.* The FOV is classified cloudy if its window channel brightness temperature is too cold (<210 K).
2) *Observed and AMSU-A predicted HIRS/3 brightness*

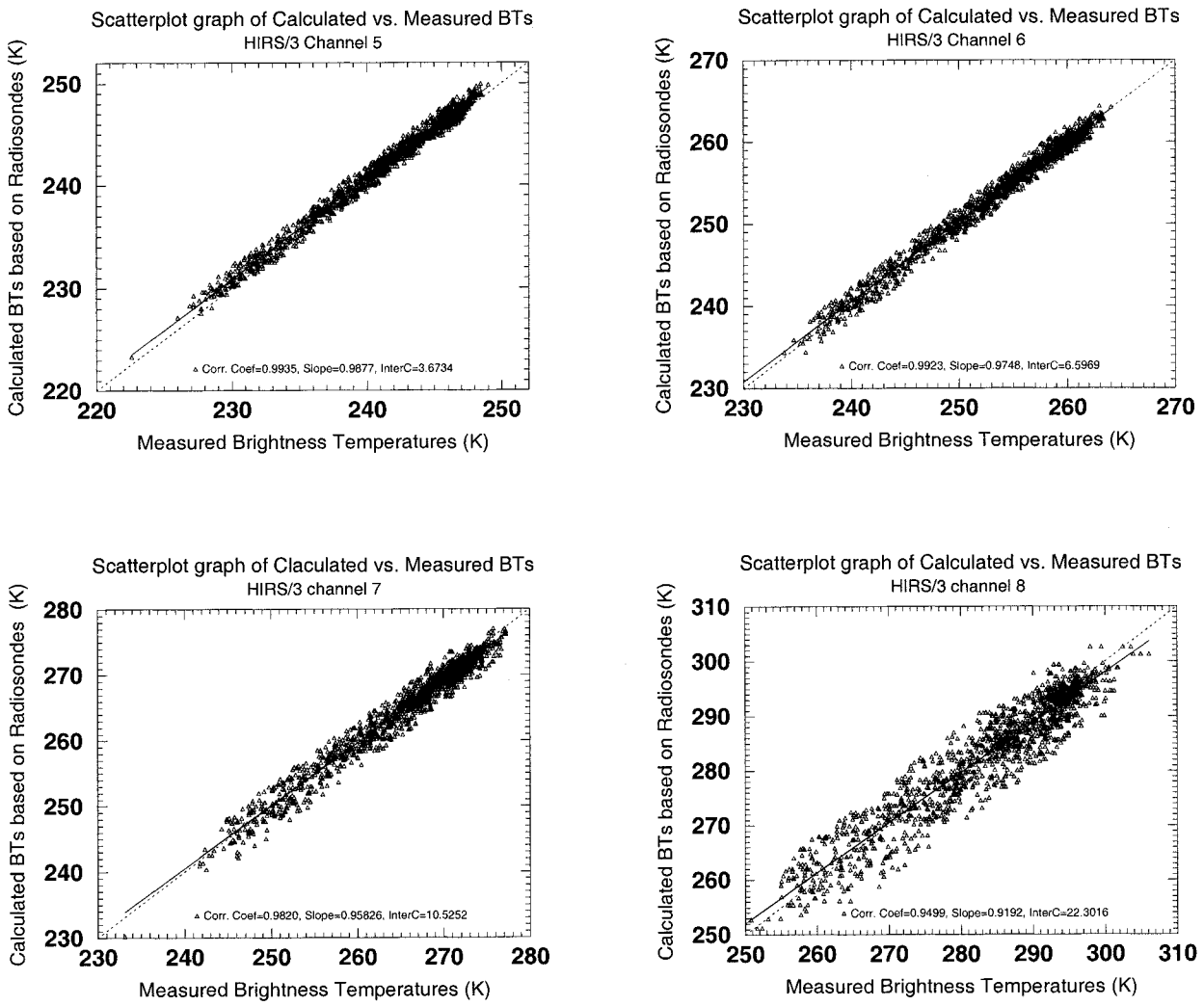


FIG. 3. Scatterplot of observed and calculated brightness temperatures for HIRS/3 channels 5, 6, 7, and 8.

*temperature difference.* In clear-sky conditions, the difference between observed and AMSU-A predicted brightness temperatures should be small for most HIRS/3 channels. However, if there is a significant discrepancy between the observed HIRS/3 and AMSU-A predicted HIRS/3 brightness temperatures for any cloud sensitive channel (4, 5, 6, 7, 13, 14, and 15), then this FOV is classified as cloudy.

3) *The warmest adjacent FOV's longwave window channel brightness temperature.* The warmest FOV is selected from its eight adjacent FOVs, if the longwave window brightness temperature is 4 K cooler than that of the warmest FOV, this FOV is classified cloudy.
4) *Multiwindow channels brightness temperature difference.* The HIRS/3 has four window channels, where three channels have a higher transparency. An atmospheric correction is calculated for each window channel and the three estimates of surface temperature are checked for consistency. If any of following checks is satisfied, then the FOV is classified as cloudy. In sunlight,

$$|\mathrm{TBO}(18) - \mathrm{TBO}(8)| > 10.0 \text{ K}.$$

At night, the test becomes

$$\mathrm{TBO}(18) - \mathrm{TBO}(8) > 2.0 \text{ K},$$

$$\mathrm{TBO}(8) - \mathrm{TBO}(18) > 4.0 \text{ K},$$

$$\mathrm{TBO}(19) - \mathrm{TBO}(18) > 2.0 \text{ K}, \quad \text{and}$$

$$\mathrm{TBO}(18) - \mathrm{TBO}(19) > 4.0 \text{ K},$$

where TBO($i$) is the brightness temperature for a given HIRS/3 channel $i$.

If there is one or more clear FOVs within the FOR, then the average of all clear FOV radiances are used for this FOR and the AMSU-A brightness temperatures are the average of all nine FOVs within this FOR. This

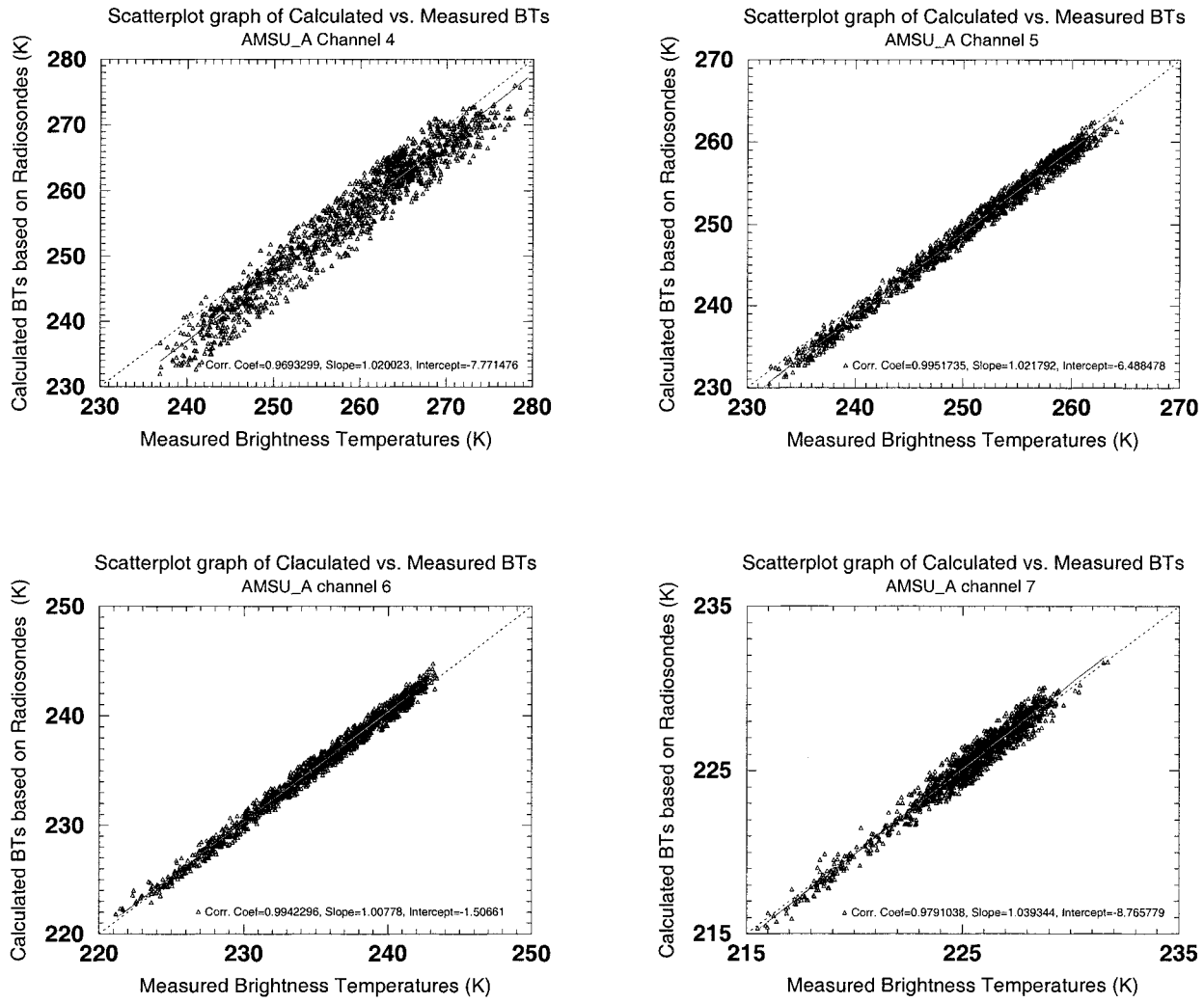


FIG. 4. Scatterplot of observed and calculated brightness temperatures for AMSU-A channels 4, 5, 6, and 7.

averaging process reduces the random noise of the measurements. However, if there is no clear HIRS/3 FOV within the FOR after the cloud screening, then a cloud removal procedure is applied to get the HIRS/3 clear column radiance from the measurements of nine cloudy FOVs. Cloud removal refers to the estimation of the radiance in the absence of clouds. We use the adjacent FOVs approach developed by Smith (1968) and Chahine (1974, 1977), which is summarized as follows.

The HIRS/3 observed radiance in a partially cloudy FOV consists of the radiance from the clear portion of the scene and radiances from the portions covered by different types of clouds. For a specific HIRS/3 channel, the radiance for a partly cloudy FOV is given by

$$R = \left(1 - \sum_{j=1}^{J} \alpha_j\right) R^{\text{clr}} + \sum_{j=1}^{J} \alpha_j R_j^{\text{cld}}, \qquad (2)$$

where $\alpha_j$ is the fraction of cloud type $j$, $R^{\text{clr}}$ is the clear column radiance for this footprint, $R_j^{\text{cld}}$ is the overcast radiance of cloud type $j$, and $J$ is number of cloud types. In the ATOVS processing, we assume that up to two layers of clouds can exist. More than two adjacent HIRS/3 FOVs are used in the cloud-removal approach for each cloud type. It is assumed that all the adjacent FOVs used in the cloud-removal procedure vary only in the cloud fractions for each cloud type; that is, all adjacent FOVs have the same $R^{\text{clr}}$ and $R_j^{\text{cld}}$ but different $\alpha_j$. The nine FOVs are sorted and grouped according to the amount of cloud (Joiner and Rokke 1998). HIRS/3 channel-8 brightness temperatures of the nine adjacent FOVs are reordered from the warmest to the coldest; then the three FOVs with the warmest, the three FOVs with the coldest, and the remaining three FOVs are averaged. This averaging reduces the noise that may be amplified in the cloud removal procedure. The cloud-removed clear column radiance for the FOR can be retrieved using the following equation:

$$\tilde{R}^{\text{clr}} = \overline{R}_1 + \eta_1(\overline{R}_1 - \overline{R}_2) + \eta_2(\overline{R}_1 - \overline{R}_3), \qquad (3)$$

TABLE 4. The coefficients for HIRS/3 and AMSU-A bias adjustment.

| HIRS/3 channel index | Slope ($a$) | Intercept ($b$) | AMSU-A channel index | Slope ($a$) | Intercept ($b$) |
|---|---|---|---|---|---|
| 1 | 0.8174493 | 43.99188 | 1* | 1.000000 | 0.000000 |
| 2 | 0.8523166 | 33.75825 | 2* | 1.000000 | 0.000000 |
| 3 | 0.8648131 | 30.56179 | 3* | 1.000000 | 0.000000 |
| 4 | 1.0282290 | −5.48383 | 4 | 1.020023 | −7.771476 |
| 5 | 0.9877007 | 3.67346 | 5 | 1.021792 | −6.488478 |
| 6 | 0.9748163 | 6.59699 | 6 | 1.007780 | −1.506610 |
| 7 | 0.9582583 | 10.52518 | 7 | 1.039344 | −8.765779 |
| 8 | 0.9191831 | 22.30155 | 8 | 0.938334 | 13.424830 |
| 9* | 1.0000000 | 0.00000 | 9 | 0.941926 | 12.654100 |
| 10 | 0.9327897 | 18.65043 | 10 | 0.932548 | 14.924470 |
| 11 | 0.8976258 | 25.74048 | 11 | 0.918347 | 18.666970 |
| 12 | 0.9241955 | 18.96372 | 12 | 0.880986 | 28.549870 |
| 13 | 0.9596393 | 9.64674 | 13 | 0.754574 | 60.506610 |
| 14 | 0.9852950 | 3.13180 | 14 | 0.682403 | 81.671510 |
| 15 | 0.9839523 | 2.04826 | 15* | 1.000000 | 0.000000 |
| 16 | 0.9921560 | 0.15154 | | | |
| 17 | 0.9578910 | 11.42773 | | | |
| 18 | 0.9329234 | 16.59371 | | | |
| 19 | 0.9020007 | 24.08484 | | | |

* Bias adjustment is not applicable for those channels.

$\overline{R}_1$ (warmest), $\overline{R}_2$, and $\overline{R}_3$ (coldest) are three averaged radiances as mentioned above, $\tilde{R}^{\text{clr}}$ is the HIRS/3 clear column radiance to be retrieved. The AMSU-A channels 6–14 are used to predict the HIRS/3 channels 4, 5, 6, and 7 clear radiances that are used to solve $\eta_1$ and $\eta_2$ using Eq. (3). Then these $\eta_1$ and $\eta_2$ are used in Eq. (3) with the cloudy radiances for each HIRS/3 channel to obtain the clear column radiances.

To illustrate the capability of the cloud removal procedure, 8834 global radiosonde profiles are used to simulate the HIRS/3 cloudy radiances and AMSU-A brightness temperatures. The instrument noise listed in Table 1 plus the assumed 0.2 K forward model error is added to the AMSU-A brightness temperatures. Figure 7 shows the root mean square error (rmse) for the AMSU-A predicted, and the cloud-removed 19 HIRS/3 channels' brightness temperatures, along with the HIRS/3 instrument noise. The regression coefficients are generated using 90% of the 8344 profiles; this coefficient is then applied to the remaining 10% of the profiles to get the rmse. This is a one-layer cloudy simulation, the average cloud amount in the simulation procedure is 56%, and the cloud pressure varies from 150∼850 millibars. From the results, it can be clearly seen that the AMSU-A measurements can predict most of the HIRS/3 channels with good accuracy. The accuracy for AMSU-A predicted HIRS/3 channels 1–3 is even better than the HIRS/3 instrument noise; this is due to the fact that AMSU-A has low instrument noise and has good sensitivity for upper tropospheric and stratospheric temperature. Although the instrument noise for HIRS/3 channels 1–3 is relatively large, the noise can be reduced by averaging radiances within the $3 \times 3$ FOVs. Therefore, these three HIRS/3 channels can be used together with AMSU-A channels to infer the upper tropospheric and stratospheric temperature information in both clear and cloudy skies.

The rmse of the AMSU-A predicted HIRS/3 brightness temperature is less than 2.0 K for channels 5–7 and 14–16 although the rmse is larger than the HIRS/3 instrument noise. These seven cloud sensitive channels are used for cloud detection in the IAPP, as described above. The rmse of the remaining AMSU-A predicted HIRS/3 channels (near surface or window channels) is much larger than the HIRS/3 instrument noise; this is due to the fact that the atmospheric information of AMSU-A measurements is limited in the near surface levels due to the radiation from the earth's surface.

The cloud-removal procedure that uses all the HIRS/3 cloudy radiances within the FOR shows a substantial improvement over the AMSU-A predicted HIRS/3 brightness temperatures, especially for those low-level and window channels (e.g., channels 7–13 and 17–19). However, the rmse of cloud-removed HIRS/3 brightness temperatures for those low-level and window channels is still about 1.0∼1.5 K. This is so-called noise amplification in the cloud removal procedure. In real data processing, multiple layer/phase clouds can occur within a HIRS/3 FOV, and it is not reliable to apply the cloud-removal technique to HIRS/3 measurements under this condition. Therefore, FOVs containing multiple layer/phase clouds need to be identified before the retrieval procedure.

## 4. First guess from linear regression retrieval

Because the retrieval problem is ill-posed, additional information is needed to constrain the solution. Often this is accomplished by means of a first-guess profile obtained from a climate mean, a regression technique,

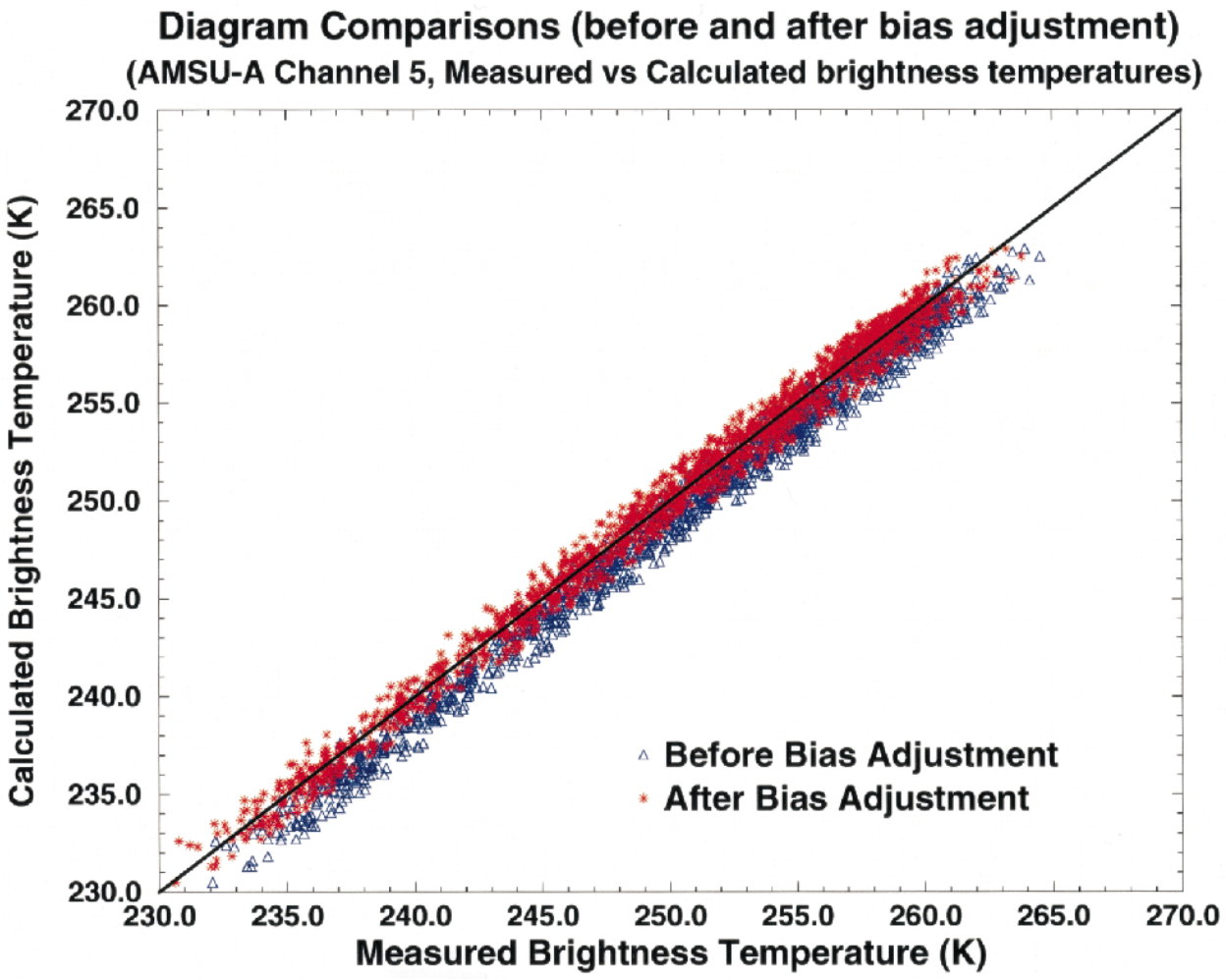


FIG. 5. Comparisons between AMSU-A channel 5 observed and calculated (from collocated radiosondes) brightness temperatures. The blue and red spots are before and after bias adjustment, respectively.

and/or numerical forecast products. The IAPP retrieval involves two steps: 1) an initial temperature, water vapor, ozone profile, and surface skin temperature is obtained by statistical regression based on the NOAA/NESDIS NOAA 88 global radiosonde dataset that has 8834 atmospheric profiles, and 2) an iterative physical solution of the radiative transfer equation is conducted using the results of step 1 as the initial profile to get the final temperature profile, moisture profile, and total atmospheric ozone. In the IAPP, a statistical regression model is generated for the first-guess retrieval from ATOVS measurements under both clear and cloudy sky conditions; the regression result is calculated for the HIRS/3 single FOV. The fast forward model calculation of AMSU-A and HIRS/3 radiance is performed for each radiosonde case of the NOAA 88 dataset to provide a radiosonde-ATOVS radiance pair for the statistical regression analysis. A regression equation is then generated based on these theoretical calculations of radiance and the matching radiosonde temperature, moisture, and ozone profiles. This regression equation can be applied to the real ATOVS radiances to generate an excellent initial profile of the atmospheric state, as needed for the physical solution of the RTE. In addition, the local satellite zenith angle of observation, the surface terrain elevation, and the land/water index are also used as predictors to allow the direct use of nonlimb adjusted radiances. Another way to generate the regression equation is by using the matchup file that contains the time and space collocated satellite radiance measurements and radiosonde profiles (Goldberg 1999). The advantage of the regression equation using the theoretical calculation over the real observation is that it avoids errors due to time and space differences between the satellite observation and radiosonde profile; however, using the real matchup data will overcome the impact of bias caused by the imperfection of forward model calculation.

Time and space collocated surface temperature and moisture observations can also be used as two additional

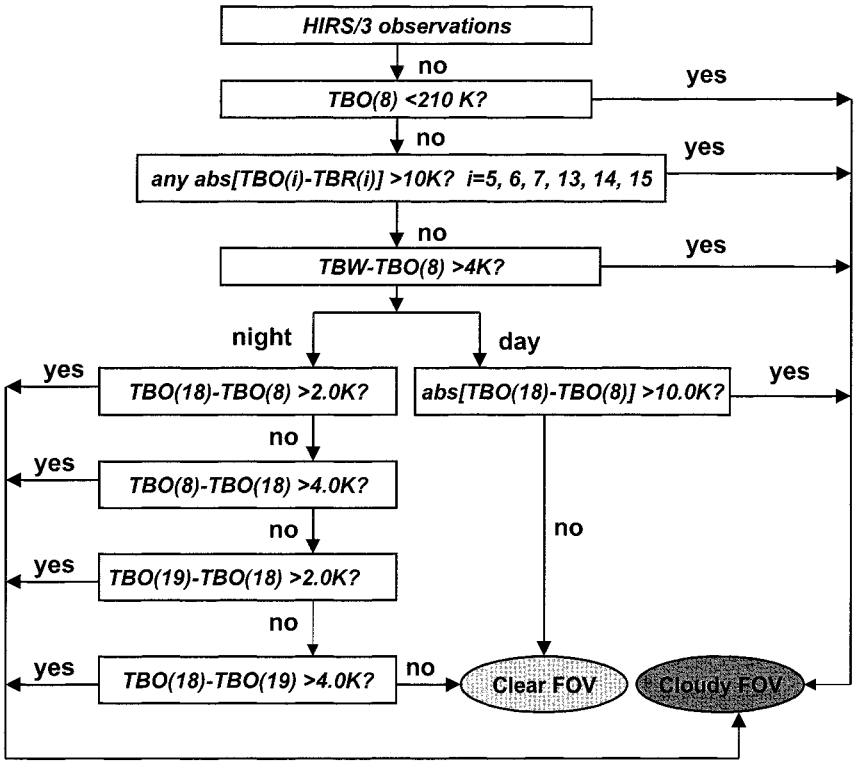


FIG. 6. An illustration of HIRS/3 cloud detection scheme. TBO represents the observed HIRS/3 brightness temperature, TBW represents the warmest adjacent FOV's longwave window channel brightness temperature, and TBR represents AMSU-A predicted HIRS/3 brightness temperature.

predictors in the regression. For example, if the hourly surface temperature and moisture observations are available within the FOR, the surface observations provide additional information to better constrain the statistical retrieval at near surface levels. Because the IAPP uses the $3 \times 3$ HIRS/3 FOVs observations to obtain one retrieval profile, the averaged HIRS/3 clear radiances and averaged AMSU-A brightness temperatures within the nine FOVs are applied to the regression equation. Under clear sky conditions, the HIRS/3 measurements plus the AMSU-A measurements are used to predict the atmospheric temperature and moisture profiles, total ozone, surface skin temperature, and microwave surface emissivity. Under cloudy sky conditions, only the AMSU-A and HIRS/3 stratospheric channel measurements are used to predict these atmospheric parameters. Because of the fact that the cloud-removal procedure amplifies measurement noise, we do not use the cloud-removed clear column radiances of HIRS/3 channels to retrieve the atmospheric temperature and moisture profiles under cloudy conditions, instead the AMSU-A and HIRS/3 channels 1–3 are used.

Atmospheric ozone is also retrieved in cloudy sky where the cloud-removed HIRS/3 clear column radiances are used. However, the accuracy is limited because of the noise amplification in the cloud-removal procedure. A first guess of the microwave surface emissivity is obtained from the AMSU-A 50.3-GHz window channel brightness temperature (Huang and Li 1998), and the emissivity of the other AMSU-A channels is determined by model calculation based on the frequency.

## 5. Physical iterative retrieval algorithm

Once the first guess is generated from the regression technique described above, a nonlinear iterative procedure is applied to the radiative transfer equation to further improve the first guess. This procedure is described here.

If we neglect scattering by the atmosphere, the true clear spectrum of infrared radiance exiting the earth–atmosphere system is approximated by

$$R = \varepsilon B_s \tau_s - \int_0^{p_s} B \, d\tau(0, p) + (1 - \varepsilon) \int_0^{p_s} B \, d\tau^* + R', \tag{4}$$

where $\tau^* = \tau_s^2/\tau$; $R$ is the spectral radiance in the infrared region or brightness temperature in the microwave region; $B$ is the Planck radiance in the infrared region or temperature in the microwave region, which is a function of pressure $p$; $\tau$ is the atmospheric trans-

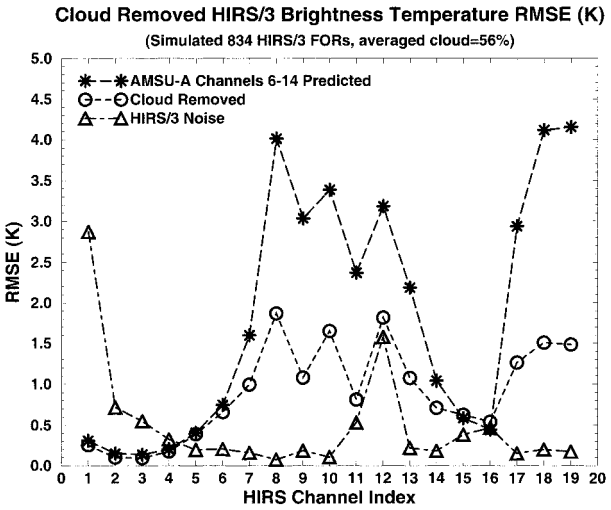


FIG. 7. Rmse of AMSU-A predicted and cloud-removed HIRS/3 brightness temperatures, plus the HIRS/3 instrument noise.

mittance function; subscript $s$ denotes surface; $R'$ represents the contribution of reflected solar radiation in the infrared region; and $\varepsilon$ is the surface emissivity (assumed to be equal to 0.99 for infrared window channel). If the satellite-observed radiance or brightness temperature $R$ of each channel is known, then $R$ can be considered a nonlinear function of the atmospheric temperature profile, water vapor mixing ratio profile, surface skin temperature, microwave surface emissivity, etc. That is, $R = R(T, q, T_s, \varepsilon, \ldots)$, or in general

$$\mathbf{Y} = \mathbf{F}(\mathbf{X}), \tag{5}$$

where the vector $\mathbf{X}$ contains $L$ (levels of atmosphere) atmospheric temperatures, $L$ atmospheric water vapor mixing ratios (the water vapor is expressed as the logarithm of the mixing ratio in practical applications), one surface skin temperature, one microwave surface emissivity, etc., and $\mathbf{Y}$ contains $N$ satellite observed radiances or brightness temperatures. The linear form of Eq. (5) is

$$\delta\mathbf{Y} = \mathbf{F}'\delta\mathbf{X}, \tag{6}$$

where $\mathbf{F}'$ is the linear or tangent model of the forward model $\mathbf{F}$. Here, $\mathbf{F}'$ is also the so-called weighting function matrix and these weighting functions can be calculated by a differential scheme or perturbation method, especially for the water vapor mixing ratio and ozone mixing ratio components. However, an accurate and efficient way to calculate the weighting functions is necessary for real-time data retrieval processing. Here the linear model $\mathbf{F}'$ uses an efficient analytical form (Li 1994); see the appendix for the derivation of the linearization form of the RTE. A general form of the minimum variance solution is to minimize the following penalty function (Rodgers 1976)

$$J(\mathbf{X}) = [\mathbf{Y}^m - \mathbf{Y}(\mathbf{X})]^{\mathrm{T}}\mathbf{E}^{-1}[\mathbf{Y}^m - \mathbf{Y}(\mathbf{X})] + (\mathbf{X} - \mathbf{X}_0)^{\mathrm{T}}\mathbf{H}(\mathbf{X} - \mathbf{X}_0). \tag{7}$$

By using the following Newtonian iteration

$$\mathbf{X}_{n+1} = \mathbf{X}_n + J''(\mathbf{X}_n)^{-1} \cdot J'(\mathbf{X}_n), \tag{8}$$

the following quasi-nonlinear iterative form (Eyre 1989) is obtained

$$\delta\mathbf{X}_{n+1} = (\mathbf{F}_n'^{\mathrm{T}} \cdot \mathbf{E}^{-1} \cdot \mathbf{F}_n' + \mathbf{H}) \cdot \mathbf{F}_n'^{\mathrm{T}} \cdot \mathbf{E}^{-1} \times (\delta\mathbf{Y}_n + \mathbf{F}_n' \cdot \delta\mathbf{X}_n), \tag{9}$$

where $\delta\mathbf{X}_n = \mathbf{X}_n - \mathbf{X}_0$, $\delta\mathbf{Y}_n = \mathbf{Y}^m - \mathbf{Y}(\mathbf{X}_n)$, $\mathbf{X}$ is the atmospheric profile to be retrieved, $\mathbf{X}_0$ is the initial state of the atmospheric profile or the first guess, $\mathbf{Y}^m$ is the vector of the observed radiances or brightness temperatures used in the retrieval process, $\mathbf{E}$ is the observation error covariance matrix that includes instrument noise and forward model error, $\mathbf{H}$ is the a priori matrix that constrains the solution, and superscript T denotes the transpose. Here, $\mathbf{H}$ can be the inverse of the a priori first-guess error covariance matrix or another type of matrix. If the statistics of both the measurement and a priori error covariance matrix are Gaussian, then the maximum likelihood solution is obtained. However, if the a priori error covariance matrix is not known or is estimated incorrectly, the solution will be suboptimal (Chahine et al. 1996). Usually $\mathbf{H} = \gamma\mathbf{I}$ is applied in Eq. (9), where $\gamma$ is the smoothing factor. Equation (9) becomes

$$\delta\mathbf{X}_{n+1} = (\mathbf{F}_n'^{\mathrm{T}} \cdot \mathbf{E}^{-1} \cdot \mathbf{F}_n' + \gamma\mathbf{I}) \cdot \mathbf{F}_n'^{\mathrm{T}} \cdot \mathbf{E}^{-1} \times (\delta\mathbf{Y}_n + \mathbf{F}_n' \cdot \delta\mathbf{X}_n). \tag{10}$$

While the smoothing factor $\gamma$ is extremely important in the solution, but it is very difficult to determine. The value $\gamma$ is dependent upon the observations, the observation error, and the first guess of the atmospheric profile; often it is chosen empirically (Susskind 1984; Smith et al. 1985; Hayden 1988). The smoothing factor plays a critical role in the solution; if $\gamma$ is too large, then the solution is overconstrained and large biases could be created in the retrieval, while if $\gamma$ is too small, the solution is less constrained and possibly unstable. In the IAPP retrieval procedure, the discrepancy principle following Li and Huang (1999), is applied to determine the smoothing factor $\gamma$. Thus

$$\|\mathbf{F}[\mathbf{X}(\gamma)] - \mathbf{Y}^m\|^2 = \sigma^2, \tag{11}$$

where $\sigma^2 = \sum_{k=1}^{N} e_k^2$, $e_k$ is the square root of the diagonal of $\mathbf{E}$ or the observation error of channel $k$, which includes instrument error and forward model error (that is $e_k^2 = \eta_k^2 + f_k^2$, where $\eta_k$ is the instrument noise of channel $k$ while $f_k$ is the forward model error for the same channel). Usually $\sigma^2$ can be estimated from the instrument noise and the validation of the atmospheric transmittance model used in the retrieval. Because Eq. (11) has a unique solution for $\gamma$ (Li and Huang 1999), with Eq. (10) and Eq. (11), the atmospheric parameters and the smoothing factor can be determined together. In the IAPP, a simple

numerical approach is adopted for solving Eq. (11), $\gamma$ is changed in each iteration according to

$$\gamma_{n+1} = q_n \gamma_n, \tag{12}$$

$q$ is a factor for $\gamma$ increasing or decreasing. Based on Eq. (11), $q$ is obtained in each iteration by the following conditions:

$$\begin{aligned} q_0 = 1; \quad &\text{if } \|\mathbf{F}(\mathbf{X}_n) - \mathbf{Y}^m\|^2 < \sigma^2 \quad \text{then } q_n = 1.5; \\ &\text{if } \|\mathbf{F}(\mathbf{X}_n) - \mathbf{Y}^m\|^2 = \sigma^2 \quad \text{then stop iteration;} \\ &\text{if } \|\mathbf{F}(\mathbf{X}_n) - \mathbf{Y}^m\|^2 > \sigma^2 \quad \text{then } q_n = 0.8. \end{aligned}$$

The $q$ factor has been found from empirical experience to ensure that the solution is stable from one iteration to the next. Then, $\gamma$ will keep changing until the iteration stops.

Because there are correlations among atmospheric variables, only a limited number of variables are needed to explain the vertical structure variations of an atmospheric profile (Smith 1976). The number of independent structure functions can be obtained from a set of global atmospheric profile samples. Assume

$$\mathbf{X} - \mathbf{X}_0 = \mathbf{\Phi A}, \tag{13}$$

where $\mathbf{A} = (\alpha_1, \alpha_2, \ldots, \alpha_M)$, and

$$\mathbf{\Phi} = \begin{bmatrix} \Phi_T & 0 & 0 & 0 & 0 \\ 0 & \Phi_q & 0 & 0 & 0 \\ 0 & 0 & \Phi_o & 0 & 0 \\ 0 & 0 & 0 & \Phi_{T_s} & 0 \\ 0 & 0 & 0 & 0 & \Phi_{\varepsilon} \end{bmatrix},$$

$\mathbf{\Phi}_T$ is the matrix of the first $\tilde{N}_T$ EOFs of the temperature profile, $\mathbf{\Phi}_q$ is the matrix of the first $\tilde{N}_q$ EOFs of the water vapor mixing ratio profiles, $\mathbf{\Phi}_o$ is the matrix of the $\tilde{N}_o$ ozone mixing ratio profiles, $\mathbf{\Phi}_{T_s} = \mathbf{\Phi}_{\varepsilon} = 1$, and $M = \tilde{N}_T + \tilde{N}_q + \tilde{N}_o + 1 + 1$. It is obvious that $\mathbf{\Phi}^{\mathrm{T}}\mathbf{\Phi} = I$. Defining $\tilde{\mathbf{F}}' = \mathbf{F}'\mathbf{\Phi}$, Eq. (10) becomes

$$\mathbf{A}_{n+1} = (\tilde{\mathbf{F}}_n'^{\mathrm{T}}\mathbf{E}^{-1}\mathbf{F}_n' + \gamma\mathbf{I})\tilde{\mathbf{F}}_n'^{\mathrm{T}}\mathbf{E}^{-1}(\delta\mathbf{Y}_n + \tilde{\mathbf{F}}_n'\mathbf{A}_n), \tag{14}$$

where $\mathbf{A}_0 = 0$. Equations (14) and (11) are applied to derive the solution from ATOVS observations.

Again, time and space collocated surface observations can also be used in the physical retrieval procedure. The surface temperature and moisture observations are treated as two additional ''channels'' of information to assist the lower atmospheric structure determination. Thus, two additional equations are added in the linearized radiative transfer equations for inversion solution (see the appendix for the details on using the ancillary surface observations).

## 6. Quality control for the retrieval processing

Several checks are made for the retrieval quality control.

### *a. Convergence check*

The following quantity is computed to check the convergence

$$\chi_i = |\mathbf{X}_i - \mathbf{X}_{i-1}|, \tag{15}$$

if $\chi_{i+1} > \chi_i$ within two iterations (which means the iteration diverges), then the iteration is stopped, and the retrieval is set to the first guess; otherwise keep iterating until $\chi < 0.25$, or a maximum of 10 iterations is reached. Usually, more than 95% of solutions obtain convergence.

### *b. Saturation check*

At each iteration, each level of the water vapor profile is checked for supersaturation. If a level is supersaturated, 100% relatively humidity is assumed.

### *c. AMSU-A cloud check*

The AMSU-A scattering index and discriminate functions (Grody 1999) are used to obtain the surface characteristics such as sea ice concentration, precipitation identification, and snow cover. The derived scattering index and rainfall index can be used to reject the retrievals. The scattering index is defined as

$$\mathrm{SI} = \begin{cases} -113.2 + (2.41 - 0.0049T23)T23 \\ \quad + 0.454T31 - T89 & \text{Water} \\ T23 - T89 & \text{Land,} \end{cases} \tag{16}$$

where $T23$, $T31$, and $T89$ are the brightness temperatures for AMSU-A channels 1, 2, and 15, respectively. If the scattering index is greater than 35, then the FOR is rejected for retrieval processing.

### *d. Water–land boundary retrieval processing*

If the FOR contains FOVs both over water and land, then the FOVs are organized into groups in order: clear water FOVs, clear land FOVs, and cloudy water FOVs. Only FOVs from the highest-order category are used in water–land boundary retrieval processing. For example, if there are clear water FOVs within the FOR, only the clear water FOVs are used in retrieval. If there is no clear water FOVs, then the clear land FOVs are used. If there is neither clear water FOVs nor clear land FOVs, then cloudy water FOVs are used.

## 7. Retrieval results: Validation and analysis

### *a. Vertical profiles*

The algorithm has been tested with ATOVS measurements; *NOAA-15* ATOVS data from 15–16 November 1998 were used in a detailed comparison between radiosonde profiles and ATOVS sounding profiles. HIRS/3 channels and AMSU-A channels are used in

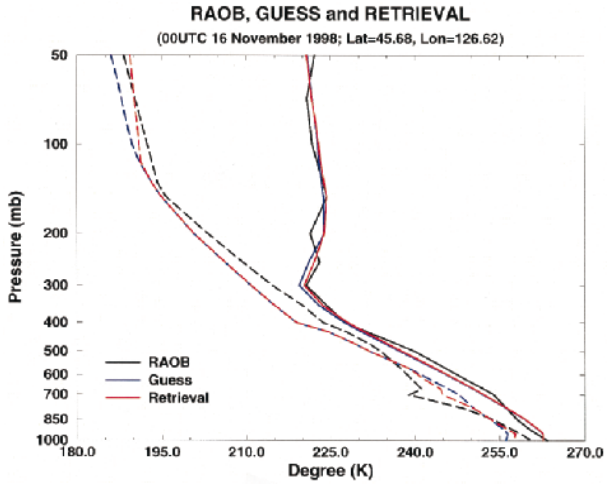


FIG. 8. Clear sky physical retrieval compared with the regression first guess and raob profile. Solid lines are for temperature and dashed lines are for dewpoint temperature. HIRS/3 and AMSU-A channels are used in the retrieval.

both regression and physical retrieval procedures in clear sky conditions while only HIRS/3 stratosphere channels 1–3 and AMSU-A channels are used in cloudy sky conditions. Only ATOVS data within 2 h of the radiosonde and 1.0° latitude/longitude (except in the polar region) are used in retrieval validation. The space distance between the ATOVS and raob measurements must be within 1.0° latitude–longitude, except in the polar region.

Several ATOVS soundings were chosen to compare with the radiosonde profiles. Those profiles include clear retrieval, cloudy retrieval, land retrieval, and ocean retrieval. Figure 8 shows a clear (HIRS/3 + AMSU-A) physical retrieval compared with the regression first guess and the raob profile. Both the regression and the physical retrieval are close to the radiosonde observation, and the physical retrieval does improve the first guess from 200 mb to 500 mb for temperature and also for some low-level water vapor. However, there is only a slight change from the first guess to the physical retrieval for temperatures below 500 mb. This means the regression retrieval has provided most of the temperature information from ATOVS low-level channels in this case. Figure 9 shows the associated HIRS/3 and AMSU-A brightness temperature residual for the same case. It can be seen that the HIRS/3 residuals for some channels are reduced significantly in iterating from the first guess to the second iteration, suggesting that the HIRS/3 measurements can influence the physical retrieval profile. There is much less significant change for AMSU-A residuals; this is due to the fact that the regression procedure can fit the temperature-sensitive AMSU-A channels well, since microwave radiances are linear functions of temperature. Figure 10 shows another clear retrieval over land. The raob exhibits fine temperature changes in the low-level atmosphere (low-level inversion near 900 mb); although the ATOVS did not resolve this fine structure, it remains close to the raob profile in the mean.

Figure 11 shows two adjacent FORs' HIRS/3 (upper

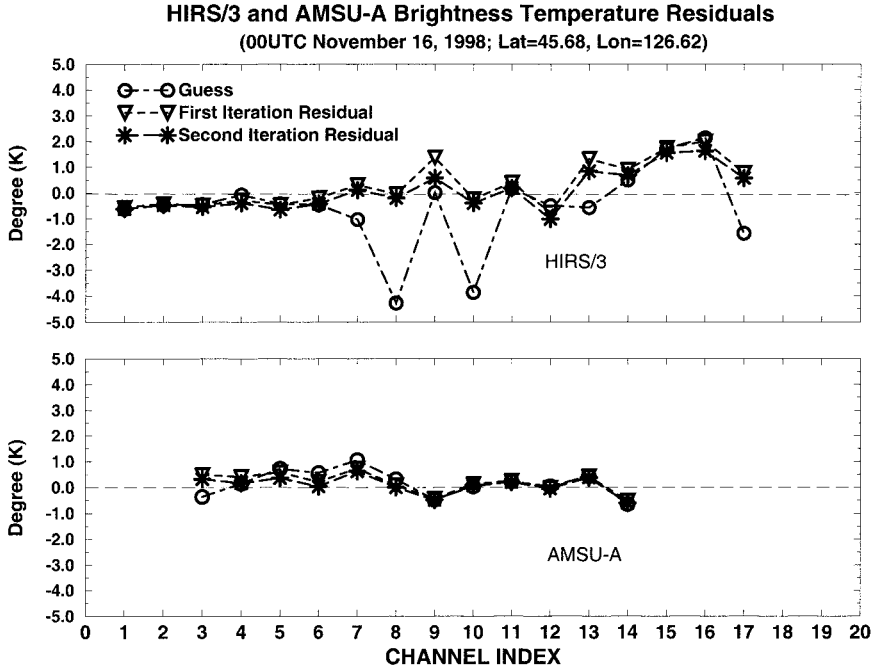


FIG. 9. HIRS/3 and AMSU-A brightness temperature residuals associated with the retrieval in Fig. 8.

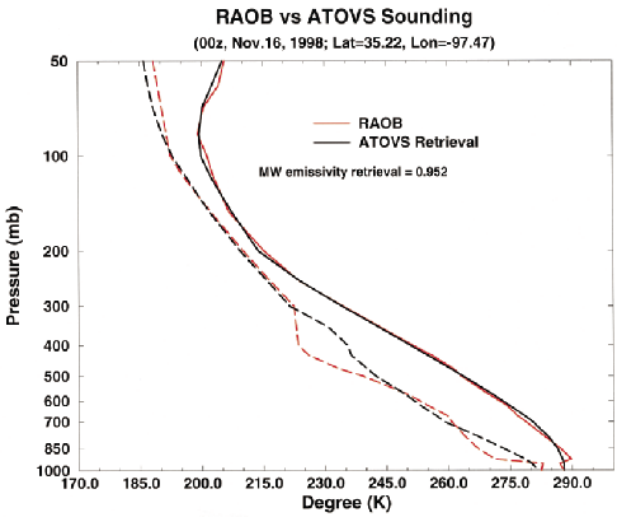


FIG. 10. Comparison of ATOVS sounding and raob profile for a clear land retrieval. HIRS/3 and AMSU-A channels are used.

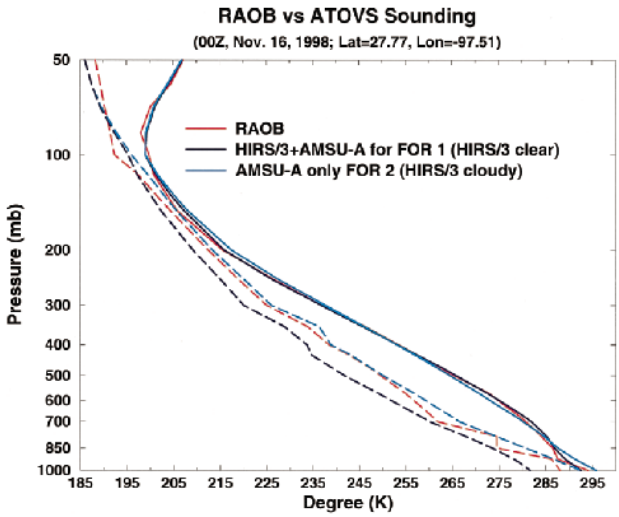


FIG. 12. Comparison of radiosonde and retrievals from the two FORs. The solid lines are for temperature profiles; the dashed lines are for dewpoint temperature profiles.

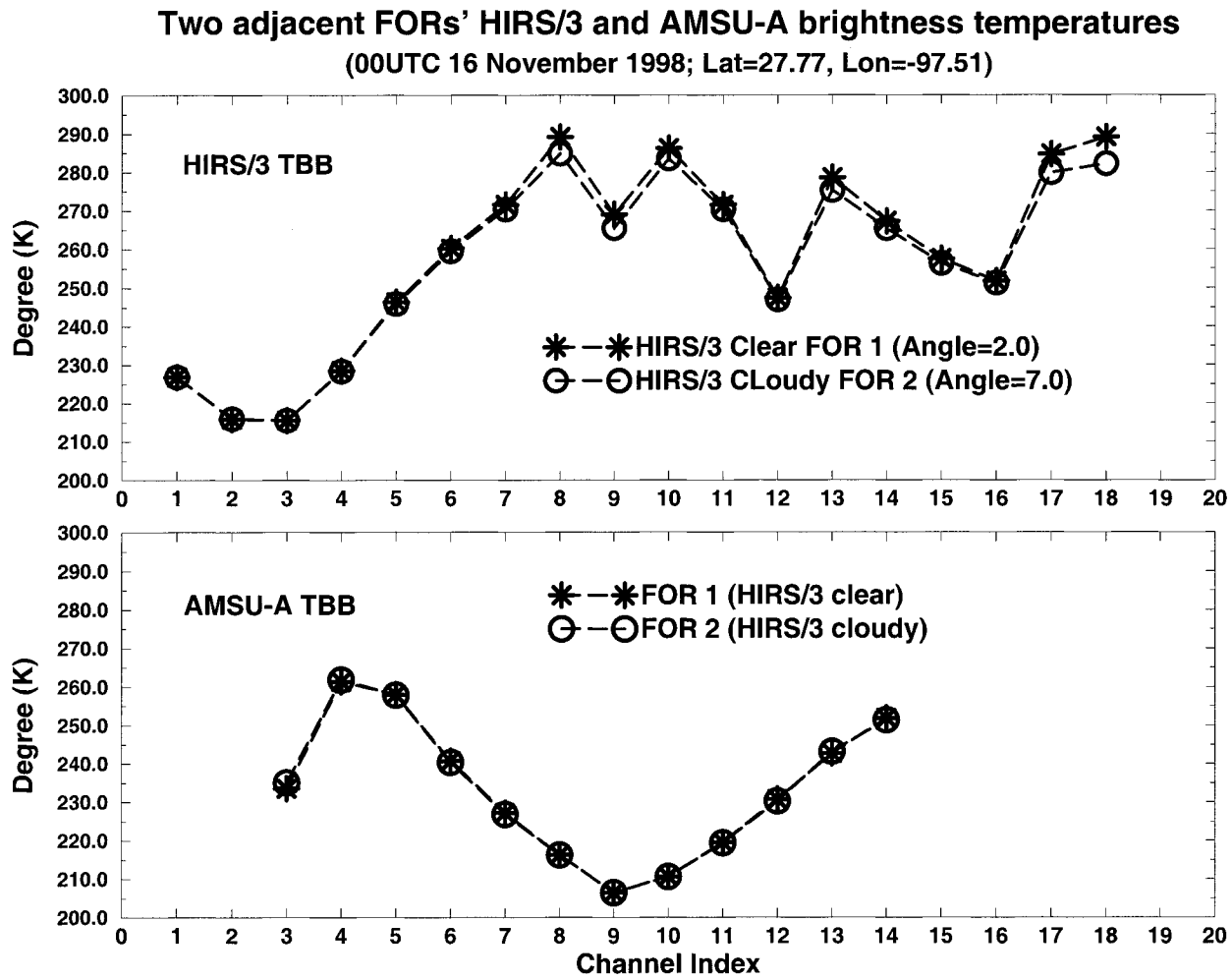


FIG. 11. HIRS/3 and AMSU-A brightness temperatures over the ocean for two adjacent FORs (one clear, the other somewhat cloudy).

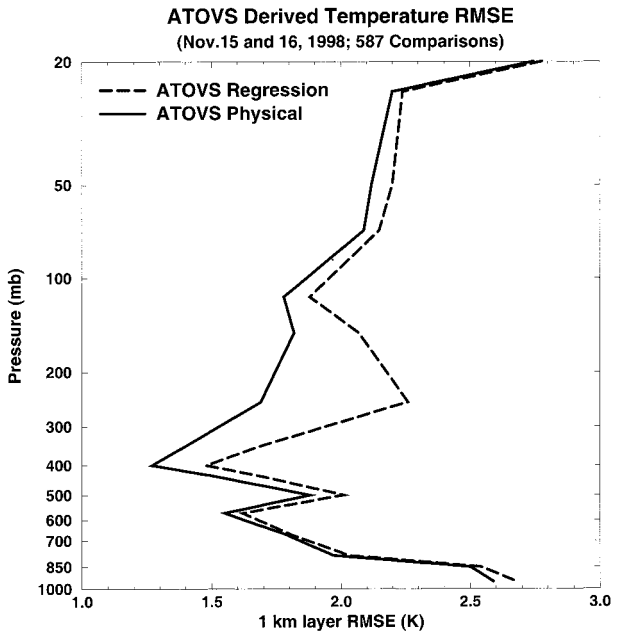


FIG. 13. One-km layer global temperature rmse of the regression and physical retrieval from 15 and 16 Nov 1998 for all clear and cloudy, land and ocean cases.

panel) and AMSU-A (lower panel) channel brightness temperatures over the ocean. The HIRS/3 window channel 8 of FOR 1 is 4.5 K warmer than that of FOR 2, the shortwave window for FOR 1 is also warmer than that of FOR 2. FOR 1 is categorized as a clear FOR while FOR 2 is categorized as a cloudy FOR after cloud

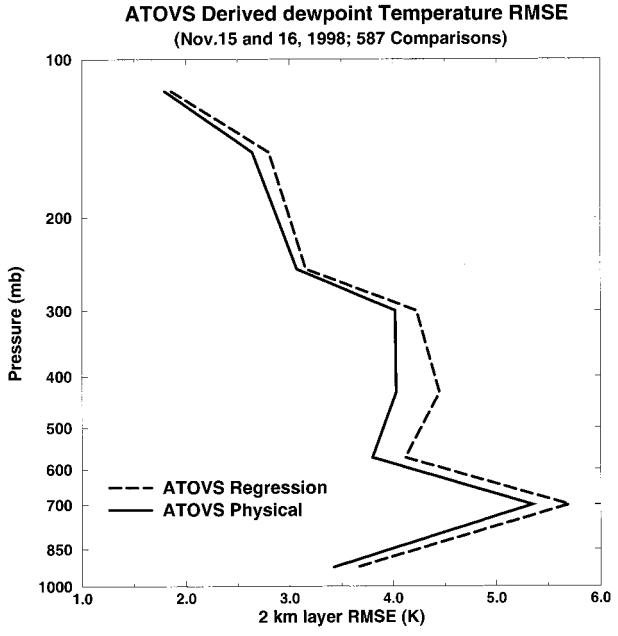


FIG. 14. Two-km layer dewpoint temperature rmse of the regression and physical retrieval from 15 and 16 Nov 1998 for all clear and cloudy, land and ocean cases.

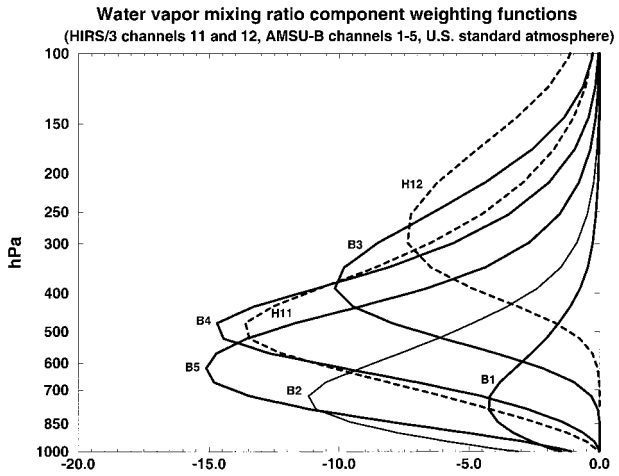


FIG. 15. The water vapor mixing ratio component weighting functions for HIRS/3 water vapor channels 11 and 12, and AMSU-B channels 1–5. The solid lines are for AMSU-B channels; the dashed lines are for HIRS/3 channels.

check procedure. There are no significant AMSU-A brightness temperature differences between the two FORs, indicating that AMSU-A is not sensitive to this cloud. For the clear FOR 1, HIRS/3 and AMSU-A measurements are used in the retrieval, while for the cloudy FOR 2, only HIRS/3 stratospheric channels and AMSU-A channels are used in the retrieval. Figure 12 shows the radiosonde profile and the retrievals from two FORs. Low-level cloud is also observed by radiosonde at 850 mb. The clear retrieval is closer in temperature to the radiosonde profile than the cloudy retrieval at the low levels and the upper troposphere. However, the clear

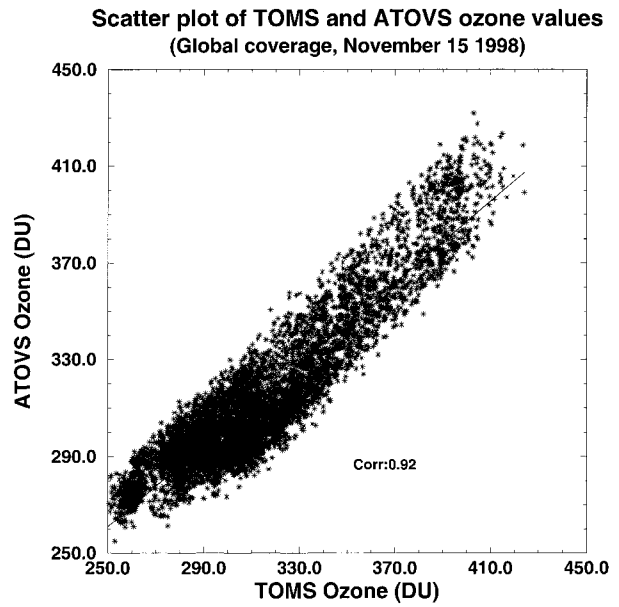


FIG. 16. Scatterplots of TOMS ozone and HIRS/3 total ozone retrievals on 15 Nov 1998.

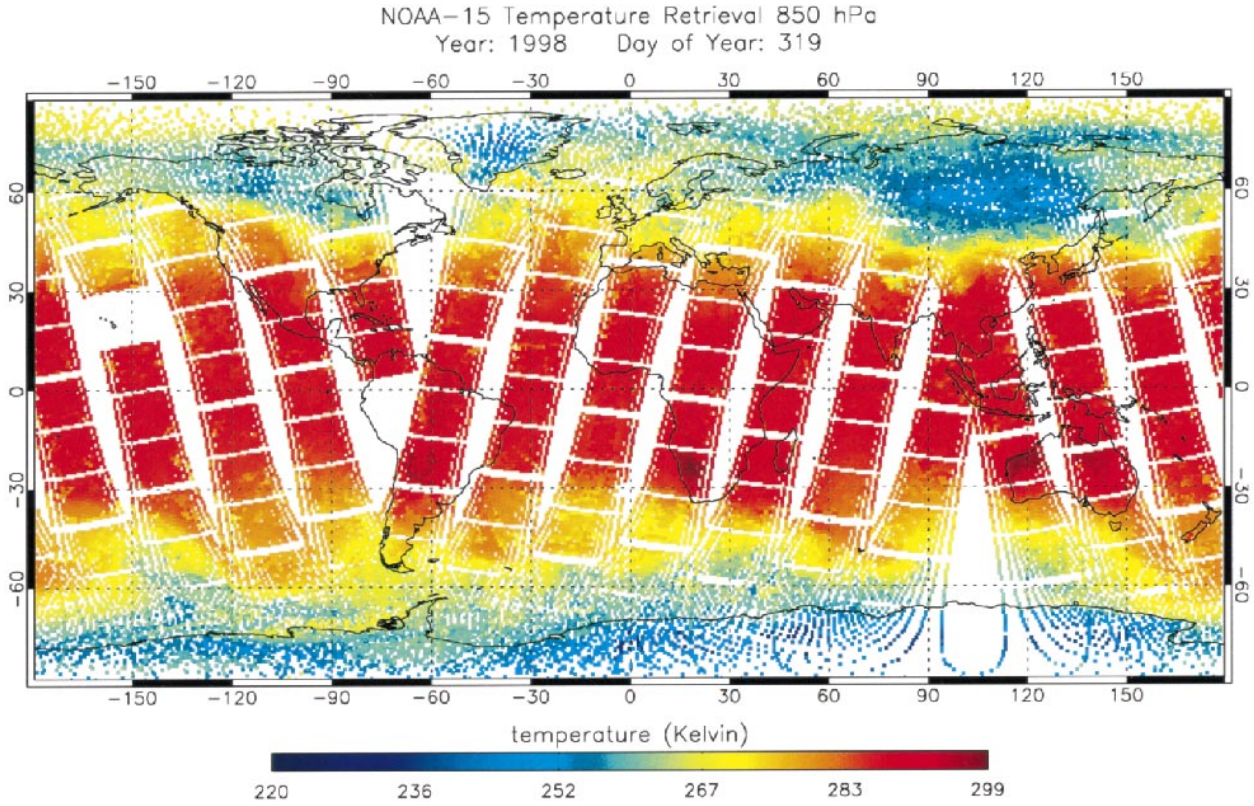


FIG. 17. Global 850-mb temperature retrievals from morning ATOVS coverage on 15 Nov 1998.

and cloudy retrievals are almost identical for the stratospheric temperature; this is due to the fact that the HIRS/3 provides almost no additional information beyond AMSU-A in the stratospheric region. For the water vapor retrieval, the AMSU-A only cloudy retrieval obtains a wetter structure at low levels, in close agreement with the radiosonde, while the HIRS/3 + AMSU-A clear retrieval is drier as one would expect for a clear FOR. Although, AMSU-A is for temperature remote sensing, channels 3–5 contain good information for boundary layer water vapor over ocean due to the low microwave surface emissivity and large contrast between the surface radiation and water vapor radiation for those channels (Zhang et al. 1999). Therefore water vapor can be retrieved over the ocean with AMSU-A only measurements.

The comparisons above show that the mean structure of atmospheric temperature and moisture profiles can be achieved from ATOVS measurements. However, because of some uncertainties, such as the failure of low-level cloud check, surface type uncertainty, emissivity error, and so on, the retrieval may be subject to a large error especially in the low atmospheric levels. In order to improve the low-level retrieval, more investigations are needed that focus on the cloud check, surface skin temperature, and the surface emissivity.

### *b. Statistical rms difference between ATOVS soundings and radiosonde observations*

A total of 587 ATOVS retrievals and collocated radiosonde observations were compared from 0000 UTC and 1200 UTC on 15 and 16 November 1998. The rmse of ATOVS retrievals is defined as

$$\text{rmse} = \sqrt{\frac{1}{N_s}\sum_{i=1}^{N_s}(X_{\text{RAOB}} - X_{\text{ATOVS}})^2}, \qquad (17)$$

where $X_{\text{RAOB}}$ and $X_{\text{ATOVS}}$ are the radiosonde observation and ATOVS retrieved parameters respectively, and $N_s$ is the total number of comparisons. Figure 13 shows the 1 km layer global temperature rmse of the regression and physical retrieval for all clear and cloudy, land and ocean cases. Results show the substantial improvement of the physical retrieval over the regression first guess especially from 100 to 500 mb. However, there is less change from the first guess for temperature below 600 mb. This is due either to the relatively large forward model error for low-level and window channels, or the failure for low-level cloud check. Usually the estimated bias for low-level and window channels from matchup data is not very good because of the error of surface skin temperature determination and the uncertainty of surface emissivity in the forward model calculation. A

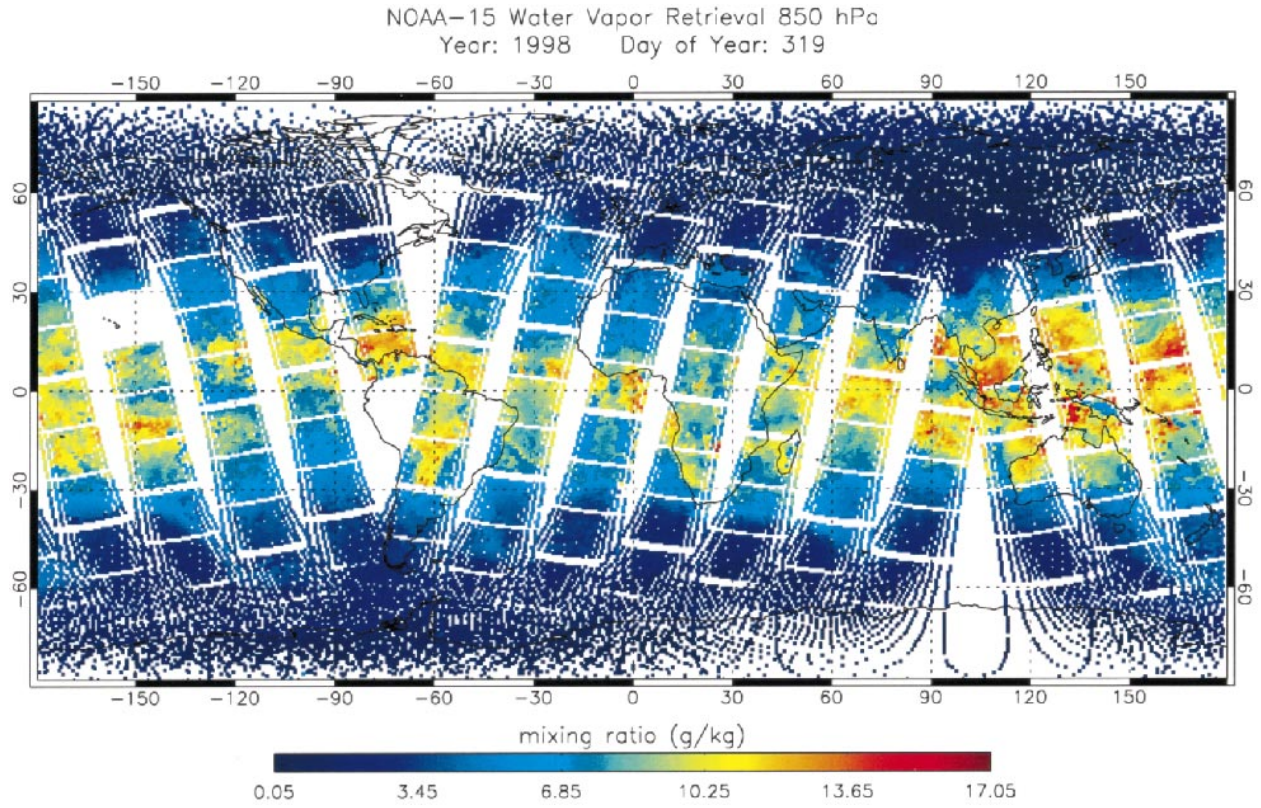


FIG. 18. Global 850-mb water vapor mixing ratio retrievals from morning ATOVS coverage on 15 Nov 1998.

relatively large forward model error still exists after bias adjustment for the low-level and window channels. This error is transferred to the low-level temperature regression retrievals. Because of the error of forward calculation in those channels, both regression and physical retrieval procedures are unable to yield all the low-level atmospheric information contained in these channels' radiance measurements. However, it should be stressed that because the iterative physical retrieval procedure is an efficient algorithm it generally improves the regression first guess, and sometimes gives substantial improvement. This physical iterative procedure is important for ATOVS data processing. The average rmse of temperature retrieval here is less than 2 K.

Figure 14 shows the 2 km layer dewpoint temperature rmse. The rmse for dewpoint temperature is less than 4 K for most layers (only 700 mb is almost 5 K). There is also improvement of the physical retrieval over the guess. With the use of AMSU-B measurements in the future, the improvement for water vapor retrieval should be more substantial. In order to demonstrate the water vapor information in AMSU-B measurements, the water vapor mixing ratio component weighting functions of HIRS/3 and AMSU-B channels are calculated based on Eq. (A.10c) in the appendix. Figure 15 shows the water vapor weighting functions for HIRS/3 water vapor channels 11 and 12, and AMSU-B channels 1–5. Because of the large instrument noise, the water vapor information is limited for HIRS/3 channel 12. AMSU-B channels 2–5 provide adequate water vapor sensitivity between 300 and 850 mb. Because of the low instrument noise, AMSU-B is expected to provide much more water vapor information than HIRS/3.

### *c. Atmospheric ozone retrievals*

Atmospheric total ozone is retrieved using HIRS/3 channel 9. The algorithm is very similar to the ozone processing used for the Geostationary Operational Environmental Satellite (GOES) sounder ozone retrieval (Li et al. 1998a). In clear sky conditions, HIRS/3 channel-9 radiance is affected by both atmospheric ozone absorption and surface skin temperature. Channel 9 is used together with other channels to obtain the total ozone retrieval. In cloudy skies, the cloud-cleared HIRS/3 clear column radiances are used for total ozone retrieval. The primary instrument used for estimating global ozone is the Total Ozone Mapping Spectrometer (TOMS) instrument (McPeters et al. 1996). TOMS is relatively insensitive to the ozone profile shape and provides high accuracy of total column ozone. However, the TOMS, which measures the backscattered ultraviolet (UV) solar radiation, cannot provide measurements in polar regions during the polar night. Ozone retrievals based on IR radiance measurements, because they do not depend on solar energy, maintain a distinct advan-

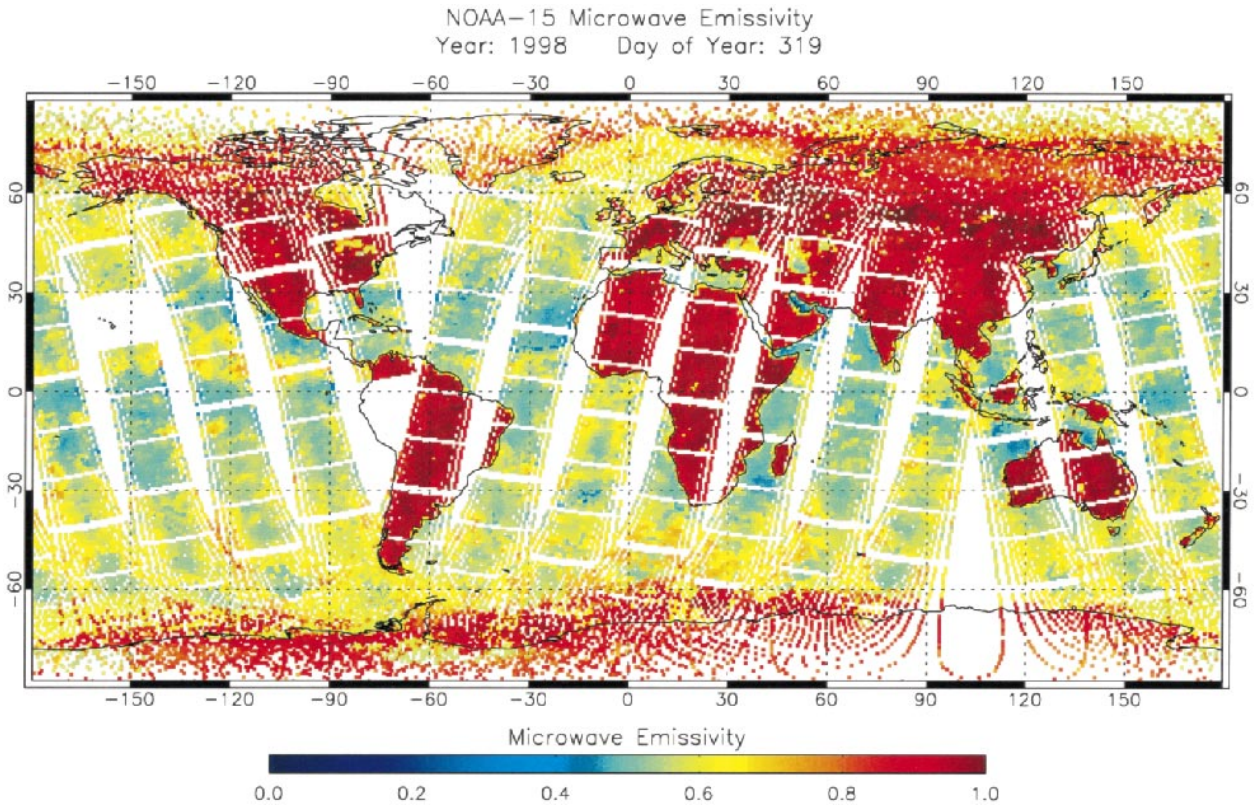


FIG. 19. Global 50.3-GHz microwave surface emissivity retrievals from morning ATOVS coverage on 15 Nov 1998.

tage over UV measurements in regions of darkness. Figure 16 shows the scattering plots of global TOMS ozone and global HIRS/3 total ozone retrievals for 15 November 1998. Only TOMS measurements from 85°N to 85°S and with solar zenith angle less than 82° are selected. The TOMS-HIRS/3 distance must be less than 0.2° latitude–longitude. Figure 16 indicates that there is good agreement between TOMS and HIRS/3 ozone measurements with an rms difference of 20 Dobson units (DU) and a correlation of 0.92.

### *d. Global images of retrievals*

With the ''all weather'' sounding capability of AMSU-A, improved global coverage in soundings can be obtained from *NOAA-15*. Figure 17 shows the 850 millibar temperatures inferred from morning ATOVS data on 15 November 1998. Scan angle corrections in retrieval have mitigated any limb darkening. Figure 18 shows the 850 mb water vapor mixing ratio retrievals. Figure 19 shows the microwave surface emissivity retrievals from AMSU-A channel at 50.3 GHz. The land and water are clearly separated in the microwave surface emissivity retrievals.

### *e. Comparison with TOVS performance*

To illustrate the improved performance of ATOVS over the TOVS system, four AMSU-A channels (3, 5, 7, and 9) that are close to the four Microwave Sounder Unit (MSU) (Smith et al. 1979) of TOVS are used to produce TOVS-like retrievals. The performance of HIRS/3 and the four selected AMSU-A channels (TOVS-like channels) should be similar to the TOVS performance (HIRS/2 + MSU). The TOVS-like measurements are used to generate the TOVS-like atmospheric sounding product. Figure 20 shows the weighting functions of the four MSU channels and AMSU-A channels 3, 5, 7, and 9, indicating that the four AMSU-A channels are close to the MSU. Figure 21 shows the 1-km vertical resolution temperature retrieval rmse from ATOVS and TOVS-like measurements on 15 and 16 November 1998. There is substantial improvement (greater than 0.2 K) of ATOVS over the TOVS-like performance above 400 hPa and below 700 hPa.

## 8. Conclusions

The IAPP algorithm designed for real-time ATOVS data processing is described in this paper; this includes the ATOVS forward model, bias correction, cloud detection and cloud-removal procedures, regression, and physical retrieval procedures. Retrieval results from the ATOVS measurements show that the algorithm is reliable under both HIRS/3 clear and cloudy conditions. Using AMSU-A measurements, the atmospheric parameters can be derived in all weather conditions with good

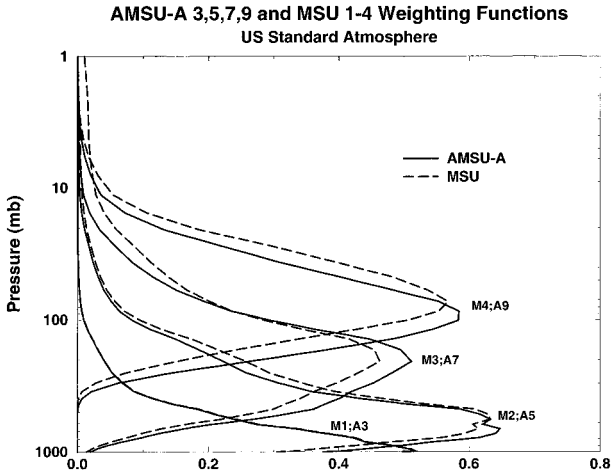


FIG. 20. Weighting functions of MSU channels and AMSU-A channels 3, 5, 7, and 9. The solid lines are for AMSU-A channels, the dashed lines are for MSU channels. ''A3'' means AMSU-A channel 3; ''M1'' means MSU channel 1.

accuracy, which is the ATOVS advantage over the previous TOVS. The retrieval validation shows that the ATOVS measurements have the accuracy of 2 K for atmospheric temperature profiles at 1-km vertical resolution and 3–6 K for dewpoint temperature profiles at 2-km vertical resolution. It is anticipated that the IAPP could be improved by including the AMSU-B measurements for water vapor profiling in the near future.

*Acknowledgments.* The authors thank H. M. Woolf and P. van Delst for the ATOVS forward model development in IAPP. C. Sisko generated the display software for IAPP retrieval products. W. L. Smith gave many good suggestions in IAPP development. Three anonymous reviewers' comments were of considerable help in improving the text and clarifying the issues. This work was conducted with support from NOAA Grant NA67ECO100 and with funds provided by licensing of the International TOVS Processing Package (ITPP), the predecessor to the IAPP.

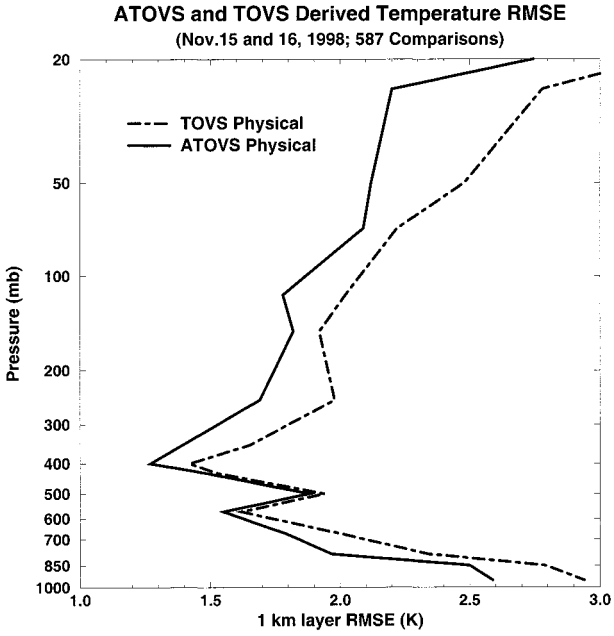


FIG. 21. One-km vertical resolution temperature retrieval rmse from ATOVS and TOVS-like measurements.

## APPENDIX

### Linearization of Radiative Transfer Equation

In this appendix the analytical linear form of RTE is derived. In the equations that follow:

$R$ = spectral radiance,
$B$ = Planck radiance which is a function of pressure level $p$,
$\tau$ = the total transmittance of the atmosphere above pressure level $p$,
$\delta(\,)$ = the difference between the true quantity and initial value denoted by a subscript 0,
$\tau_w$ = water vapor component transmittance,
$q$ = mixing ratio of water vapor,
$T$ = temperature of atmosphere at pressure level $p$,
$T_B$ = the brightness temperature,
$T_s$ = surface skin temperature,
$T_a$ = surface air temperature, and
$\varepsilon$ = infrared or microwave surface emissivity.

The RTE presented in Eq. (4) is rewritten as

$$R = \varepsilon B_s \tau_s - \int_0^{p_s} B\, d\tau(0, p) + (1 - \varepsilon) \int_0^{p_s} B\, d\tau^* + R', \qquad \text{(A1)}$$

where $\tau^* = \tau_s^2/\tau$. Hereinafter we always omit the spectrum symbol $\nu$ or channel index, and we also ignore the solar contamination for most HIRS/3 channels. Following Li (1994), the first-order variation of Eq. (A1) yields

$$\delta R = \varepsilon \tau_s \delta B_s + \varepsilon B_s \delta \tau_s - \int_0^{p_s} \delta B\, d\tau - \int_0^{p_s} B\, d\delta\tau + (1 - \varepsilon) \int_0^{p_s} \delta B\, d\tau^* + (1 - \varepsilon) \int_0^{p_s} B\, d\delta\tau^* + \left( B_s \tau_s - \int_0^{p_s} B\, d\tau^* \right) \delta\varepsilon. \qquad \text{(A2)}$$

Because

$$\int_0^{p_s} B\, d\delta\tau = B_a \delta\tau_s - \int_0^{p_s} \delta\tau\, dB, \text{ and} \qquad \text{(A3)}$$

$$\int_0^{p_s} B\, d\delta\tau^* = B_a \delta\tau_s - \int_0^{p_s} \delta\tau^*\, dB, \qquad \text{(A4)}$$

substituting Eqs. (A3) and (A4) into Eq. (A2) we have

$$\delta R = \varepsilon\tau_s\delta B_s - \int_0^{p_s} \delta B\,[d\tau - (1-\varepsilon)d\tau^*] + \varepsilon(B_s - B_a)\delta\tau_s + \int_0^{p_s} \delta\tau\, dB - (1-\varepsilon)\int_0^{p_s} \delta\tau^*\, dB + \left(B_s\tau_s - \int_0^{p_s} B\, d\tau^*\right)\delta\varepsilon. \quad \text{(A5)}$$

Following Li (1994),

$$\delta\tau = \tau\int_0^{p} \delta\,\ln q\; d\,\ln\tau_w, \quad \text{(A6)}$$

$$\delta\tau^* = (2\tau_s\delta\tau_s - \tau^*\delta\tau)/\tau = 2\tau^*\int_0^{p_s} \delta\,\ln q\; d\,\ln\tau_w - \tau^*\int_0^{p} \delta\,\ln q\; d\,\ln\tau_w, \quad \text{(A7)}$$

substituting Eq. (A6) and Eq. (A7) into Eq. (A5), we have

$$\delta R = \varepsilon\tau_s\delta B_s - \int_0^{p_s} \delta B\,[d\tau - (1-\varepsilon)d\tau^*] + \int_0^{p_s} \delta\,\ln q\left[\varepsilon(B_s - B_a)\tau_s - 2(1-\varepsilon)\int_0^{p_s} \tau^*\, dB + \int_p^{p_s} [\tau + (1-\varepsilon)\tau^*]\, dB\right] d\,\ln\tau_w + \left(B_s\tau_s - \int_0^{p_s} B\, d\tau^*\right)\delta\varepsilon \quad \text{(A8)}$$

Using the first-order variation $\delta B = (\partial B/\partial T)\,\delta T$, and assuming that $\delta R = (\partial R/\partial T_B)\,\delta T_B$, and denoting that $\beta(p) = (\partial B/\partial T)/(\partial R/\partial R_B)$ Eq. (A8) can be written as

$$\delta T_B = \beta_s\varepsilon\tau_s\delta T_s - \int_0^{p_s} \beta\left[\frac{\partial\tau}{\partial p} - (1-\varepsilon)\frac{\partial\tau^*}{\partial p}\right]\delta T\, dp + \int_0^{p_s} \delta\,\ln q\left\{(T_s - T_a)\beta_s\varepsilon\tau_s - 2(1-\varepsilon)\int_0^{p_s} \beta\tau^*\frac{\partial T}{\partial p}\, dp + \int_p^{p_s} [\beta\tau + \beta(1-\varepsilon)\tau^*]\frac{\partial T}{\partial p}\, dp\right\}\frac{\partial\,\ln\tau_w}{\partial p}\, dp + \left(\beta_s T_s\tau_s - \int_0^{p_s} \beta T\frac{\partial\tau^*}{\partial p}\, dp\right)\delta\varepsilon = W_{T_s}\delta T_s + \int_0^{p_s} W_T\delta T\, dp + \int_0^{p_s} W_q\delta\,\ln q\, dp + W_\varepsilon\delta\varepsilon \quad \text{(A9)}$$

where

$$W_{T_s} = \beta_s\varepsilon\tau_s, \quad \text{(A10a)}$$

$$W_T = -\beta\frac{\partial\tau}{\partial p} + \beta(1-\varepsilon)\frac{\partial\tau^*}{\partial p}, \quad \text{(A10b)}$$

$$W_q = \left[(T_s - T_a)\varepsilon\tau_s\beta_s - 2(1-\varepsilon)\int_0^{p_s} \beta\tau^*\frac{\partial T}{\partial p}\right]\frac{\partial\,\ln\tau_w}{\partial p} + \left\{\int_p^{p_s} \beta[\tau + (1-\varepsilon)\tau^*]\frac{\partial T}{\partial p}\right\}\frac{\partial\,\ln\tau_w}{\partial p}, \quad \text{(A10c)}$$

$$W_\varepsilon = \beta_s T_s\tau_s - \int_0^{p_s} \beta T\frac{\partial\tau^*}{\partial p}\, dp, \quad \text{(A10d)}$$

$W_{T_s}$, $W_T$, $W_q$, and $W_\varepsilon$ are called weighting functions of surface skin temperature, atmospheric temperature profile, atmospheric moisture profile, and microwave surface emissivity, respectively. The weighting function of the atmospheric ozone profile is similar to that of moisture. For IR channels, $W_\varepsilon = 0$; for microwave channels $\beta = 1$. The weighting functions are easy to calculate

for an atmospheric state. The microwave emissivity is retrieved from 50.3-GHz measurements and the emissivity of other microwave channels is derived by extrapolating based on the microwave frequency.

If ancillary surface temperature and moisture observations are available, two additional equations can be added as the following forms

$$T_{\text{obs}} - T^0(p_s) = W_{T_s}^{T_{\text{obs}}}\delta T_s + W_T^{T_{\text{obs}}}\delta T + W_q^{T_{\text{obs}}}\delta \ln q + W_\varepsilon^{T_{\text{obs}}}\delta\varepsilon, \quad \text{(A11)}$$

and

$$\ln q_{\text{obs}} - \ln q^0(p_s) = W_{T_s}^{q_{\text{obs}}}\delta T_s + W_T^{q_{\text{obs}}}\delta T + W_q^{q_{\text{obs}}}\delta \ln q + W_\varepsilon^{q_{\text{obs}}}\delta\varepsilon, \quad \text{(A12)}$$

where $T_{\text{obs}}$ and $q_{\text{obs}}$ are surface temperature and water vapor mixing ratio observations, respectively,

$$W_{T_s}^{T_{\text{obs}}} = W_q^{T_{\text{obs}}} = W_\varepsilon^{T_{\text{obs}}} = 0 \quad \text{and} \quad \begin{cases} W_T^{T_{\text{obs}}} = 1 & p = p_s \\ W_T^{T_{\text{obs}}} = 0 & p \neq p_s, \end{cases}$$

$$W_{T_s}^{q_{\text{obs}}} = W_T^{q_{\text{obs}}} = W_\varepsilon^{q_{\text{obs}}} = 0 \quad \text{and} \quad \begin{cases} W_q^{q_{\text{obs}}} = 1 & p = p_s \\ W_q^{q_{\text{obs}}} = 0 & p \neq p_s. \end{cases}$$

These two equations can be used along with Eq. (A9) in the solution. The error assumed in matrix $E$ of Eq. (10) or Eq. (14) is 1.0 K for surface temperature observation and 10% for moisture surface observation.

## REFERENCES


Chahine, M. T., 1974: Remote sounding of cloudy atmospheres. I. The single cloud layer. *J. Atmos. Sci.,* **31,** 233–243.

——, 1977: Remote sounding of cloudy atmospheres. II. Multiple cloud formations. *J. Atmos. Sci.,* **34,** 744–757.

——, and Coauthors, 1996: AIRS-team unified retrieval for core products. *Algorithm Theoretical Basis Document,* JPL, National Aeronautics and Space Administration, 106 pp.

Eyre, J. R., 1989: Inversion of cloudy satellite sounding radiances by nonlinear optimal estimation. I: Theory and simulation for TOVS. *Quart. J. Roy. Meteor. Soc.,* **115,** 1001–1026.

Fleming, H. E., P. S. Crosby, and A. C. Neuendorffer, 1986: Correction of satellite temperature retrieval errors due to errors in atmospheric transmittances. *J. Climate Appl. Meteor.,* **25,** 869–882.

Goldberg, M., 1999: AMSU-A antenna temperature adjustments, limb adjustments, and retrievals. *Tech. Proc. 10th Int. TOVS Study Conf.,* Boulder, CO, WMO and Cosponsors, 219–229.

Grody, N., 1999: Application of AMSU for obtaining water vapor cloud liquid water, precipitation, and surface measurements. *Tech. Proc. 10th Int. TOVS Study Conf.,* Boulder, CO, WMO and Cosponsors, 230–240.

Hannon, S., L. L. Strow, and W. W. McMillan, 1996: Atmospheric infrared fast transmittance models: A comparison of two approaches. *Proc. SPIE—Int. Soc. Opt. Eng.,* **2830,** 94–105.

Hayden, C. M., 1988: GOES-VAS simultaneous temperature–moisture retrieval algorithm. *J. Appl. Meteor.,* **27,** 705–733.

Huang, H.-L., and J. Li, 1998: Determination of microwave emissivity from advanced microwave sounder unit measurements. *Proc. SPIE—Int. Soc. Opt. Eng.,* **3503,** 233–237.

Joiner, J., and L. Rokke, 1998: Variational cloud clearing with TOVS data. Office Note Series on Global Modeling and Data Assimilation, GSFC, National Aeronautics and Space Administration, DAO Office Note 98-03.

Li, J., 1994: Temperature and water vapor weighting functions from radiative transfer equation with surface emissivity and solar reflectivity. *Adv. Atmos. Sci.,* **11,** 421–426.

——, and H. L. Huang, 1999: Retrieval of atmospheric profiles from satellite sounder measurements using the discrepancy principle. *Appl. Opt.,* **38,** 916–923.

——, F. X. Zhou, and Q. C. Zeng, 1994: Simultaneous non-linear retrieval of atmospheric temperature and absorbing constituent profile from satellite infrared radiances. *Adv. Atmos. Sci.,* **11,** 128–138.

——, J. P. Nelson, T. J. Schmit, W. P. Menzel, C. C. Schmidt, and H.-L. Huang, 1998a: Retrieval of total atmospheric ozone from GOES sounder radiance measurements with high spatial and temporal resolution. *Proc. SPIE—Int. Soc. Opt. Eng.,* **3501,** 291–230.

——, W. Wolf, H.-L. Huang, W. P. Menzel, P. van Delst, H. M. Woolf, and T. H. Achtor, 1998b: International ATOVS processing package: Algorithm design and its preliminary performance. *Proc. SPIE—Int. Soc. Opt. Eng.,* **3501,** 196–206.

McMillin, L. M., and C. Dean, 1982: Evaluation of a new operational technique for producing clear radiances. *J. Appl. Meteor.,* **21,** 1005–1014.

McPeters, R. D., and Coauthors, 1996: *Nimbus-7* Total Ozone Mapping Spectrometer (TOMS) data products user's guide. NASA Reference Publication, Vol. 1384, 67 pp.

Rodgers, C. D., 1976: Retrieval of atmospheric temperature and composition from remote measurements of thermal radiation. *Rev. Geophys. Space Phys.,* **14,** 609–624.

Smith, W. L., 1968: An improved method for calculating tropospheric temperature and moisture from satellite radiance measurements. *Mon. Wea. Rev.,* **96,** 387–396.

——, and H. M. Woolf, 1976: The use of eigenvectors of statistical covariance matrices for interpreting satellite sounding radiometer observations. *J. Atmos. Sci.,* **33,** 1127–1140.

——, ——, C. M. Hayden, D. C. Wark, and L. M. McMillin, 1979: TIROS-N operational vertical sounder. *Bull. Amer. Meteor. Soc.,* **60,** 1177–1187.

——, ——, ——, and A. J. Schreiner, 1985: The simultaneous export retrieval package. *Tech. Proc. Second Int. TOVS Study Conf.,* Igls, Austria, CIMSS, 224–253.

Susskind, J., J. Rosenfield, D. Reuter, and M. T. Chahine, 1984: Remote sensing of weather and climate parameters from HIRS2/MSU on TIROS-N. *J. Geophys. Res.,* **89,** 4677–4697.

Zhang, W., W. P. Menzel, and J. Li, 1999: Boundary layer and total water vapor retrieval from AMSU: Simulation study and data analysis. *Tech. Proc. 10th Int. TOVS Study Conf.,* Boulder, CO, WMO and Cosponsors, 574–585.